CHAPTER IV

RESULTS AND DISCUSSION

4.1 Parameters Affecting Formation of Al-MCM-41

4.1.1 Effect of Silica Source on Formation of Al-MCM-41

Huang *et al.* [79] proposed two-step crystallization for synthesizing MCM-41/ZSM-5 using mixed templates CTMABr, the pore-directing agent for MCM-41, and TPABr, the pore-directing agent for ZSM-5. Considering the method, in the first step crystallization, the formation of MCM-41 nucleation centers was initiated at 100°C for 2 days but the MCM-41 crystallization was not completed yet within the first 2 days. The temperature was thus raised to 150°C in the second step crystallization with lowering pH to form ZSM-5 along with MCM-41. The two-step crystallization allowed formation of MCM-41 structure in a shorter period than other methods [52]. It is known that the higher the temperature, the crystallization time is reduced. However, the temperature of 150°C certainly caused some damage of MCM-41 structure. Therefore, in our method the crystallization temperatures of 100°C for 2 days and 125°C with daily pH adjustment for further 6 days were utilized with only one type of template, i.e. CTMABr.

Different SiO_2 sources were also used in comparison. Three Al-MCM-41 samples were synthesized with the same Si/Al ratio in gel of 20: Sample SS-20 prepared from sodium metasilicate pentahydrate, Sample CS-20 from colloidal silica in the absence of NaOH solution, and Sample CS-Na-20 from a mixture of colloidal silica and NaOH solution. The XRD patterns of those samples are shown in Figure 4.1. The XRD pattern of Sample CS-20 in Figure 4.1(A) shows no reflection peaks indicating amorphous product was obtained. XRD patterns of Sample SS-20 and Sample CS-Na-20 in Figure 4.1(B) and (C), respectively, show three characteristic peaks of MCM-41 structure similar to that reported by Beck *et al.* [52]. The gel mixture prepared from colloidal silica without NaOH addition has lower pH value or alkalinity than that with NaOH addition. The latter is able to transform to Al-MCM-

41 structure while the former is not. Sodium metasilicate is also able to form Al-MCM-41 structure even at lower intensities of XRD peaks, i.e. lower crystallinity. The results show that the alkalinity effect is more pronounced than the effect of type of silica sources on the formation of Al-MCM-41.

The most intense peak observed for Samples SS-20 and Sample CS-Na-20 at 2θ of 2.2° ascribes to the reflection on (100) lattice plane and the weak intensity peaks at 2θ of 3.7° and 4.3° correspond to the reflection of (110) and (200) planes of hexagonal MCM-41 [80], respectively. The peak shift implies incorporation of aluminum in the framework of MCM-41. The decrease in peak intensities shows the less ordered structure.

4.1.2 Effect of Crystallization Time on Formation of Al-MCM-41

Figure 4.2 shows the XRD patterns of sample prepared by varying crystallization time from 6-10 days at the second step of crystallization at the temperature of 125°C, using Sample SS-20. All XRD patterns in Figure 4.2 show three characteristic peaks of Al-MCM-41 with similar crystallinity except the sample crystallized for 10 days having lower crystallinity than others. Too long period of crystallization time results in phase transformation of the metastable Al-MCM-41 toward unrequired amorphous phase. This is common for hydrothermal synthesis that the transformation of a material in the mother liquor toward another phase will occur if the product is not separated from the mother liquor within an appropriate time. Considering Figure 4.2, Sample SS-20 crystallized at 125°C for 6 days has the highest crystallinity with the narrowest peak width. Therefore, the rest of study utilized the set of samples prepared by crystallization at 125°C for 6 days after first-step crystallized at 100°C for 2 days.

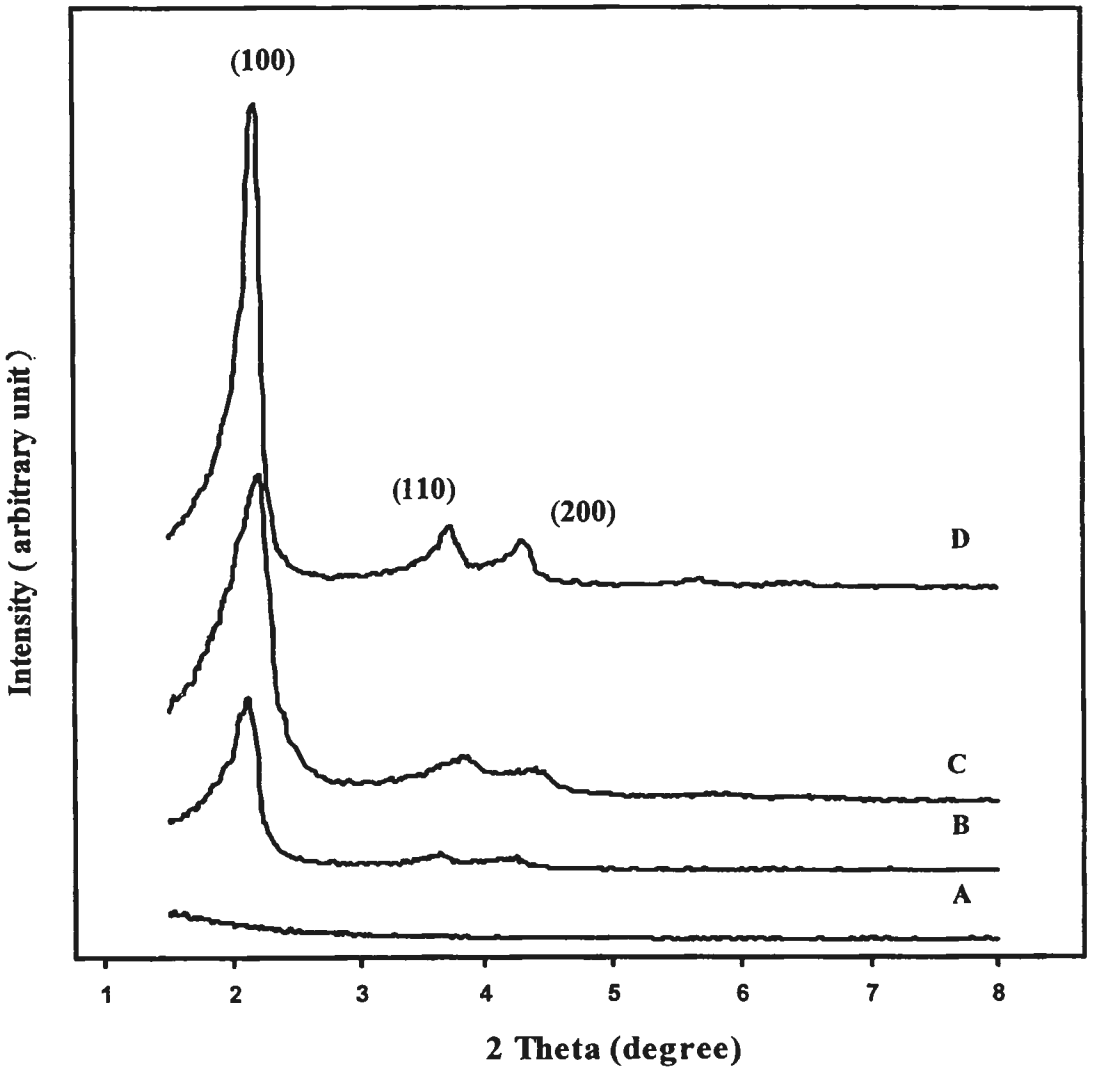

Figure 4.1 XRD patterns of the calcined samples prepared from different silica sources: (A) Sample CS-20; (B) Sample SS-20; (C) Sample CS-Na-20 and (D) Si-MCM-41.

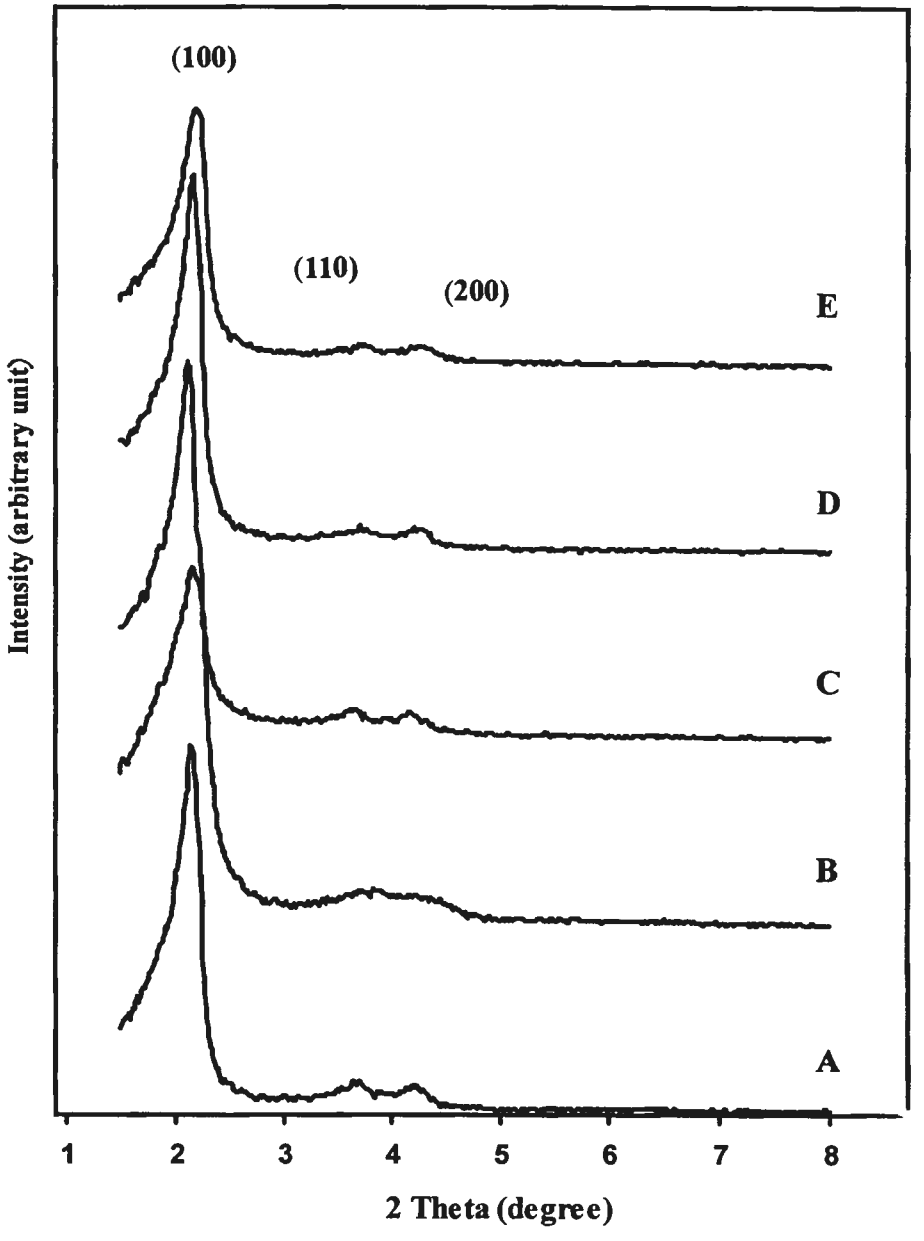

Figure 4.2 XRD patterns of the calcined SS-20 samples crystallized at the second step for various periods: (A) 6 days; (B) 7 days; (C) 8 days; (D) 9 days; (E) 10 days.

4.2 Effect of the Si/Al Ratios on Formation of Al-MCM-41

4.2.1 Elemental Analysis

The Si/Al ratios in gel and in catalyst of Sample CS-Na are compared in Table 4.1. It is acceptable that the Si/Al ratios in catalyst are roughly close to the Si/Al ratios in gel. The result suggests that the catalysts obtained really contain aluminum.

Table 4.1 Si/Al molar ratios in gel and in catalyst of calcined Sample CS-Na with different Si/Al ratios

Sample	Si/Al molar ratio in gel [a]	Si/Al molar ratio in catalyst [b]
CS-Na-20	20	22.5
CS-Na-40	40	42.0
CS-Na-80	80	76.8

a: calculated from reagent quantities.

b: Aluminum (Al) was determined by ICP-AES and Si was calculated from the deduction of AlO_2 from the sample weight.

4.2.2 XRD Results

XRD patterns of Sample CS-Na with different Si/Al ratios in gel were presented in Figure 4.3. They clearly exhibit three well-resolved XRD peaks corresponding to a hexagonal structure. When the Si/Al ratio increases, the intensity of the (100) reflection peak increases. This result suggests the incorporation of aluminum atoms because the structure becomes less ordered as increasing aluminum content.

XRD patterns of as-synthesized and calcined Sample CS-Na-20 as shown in Figure 4.4. For the calcined sample, the intensity of the peaks become two-fold stronger while each peak shifts toward a higher 2θ value. This is common for porous materials synthesized using template. The template removal from the MCM-41 channels results in the decrease of the lattice parameter.

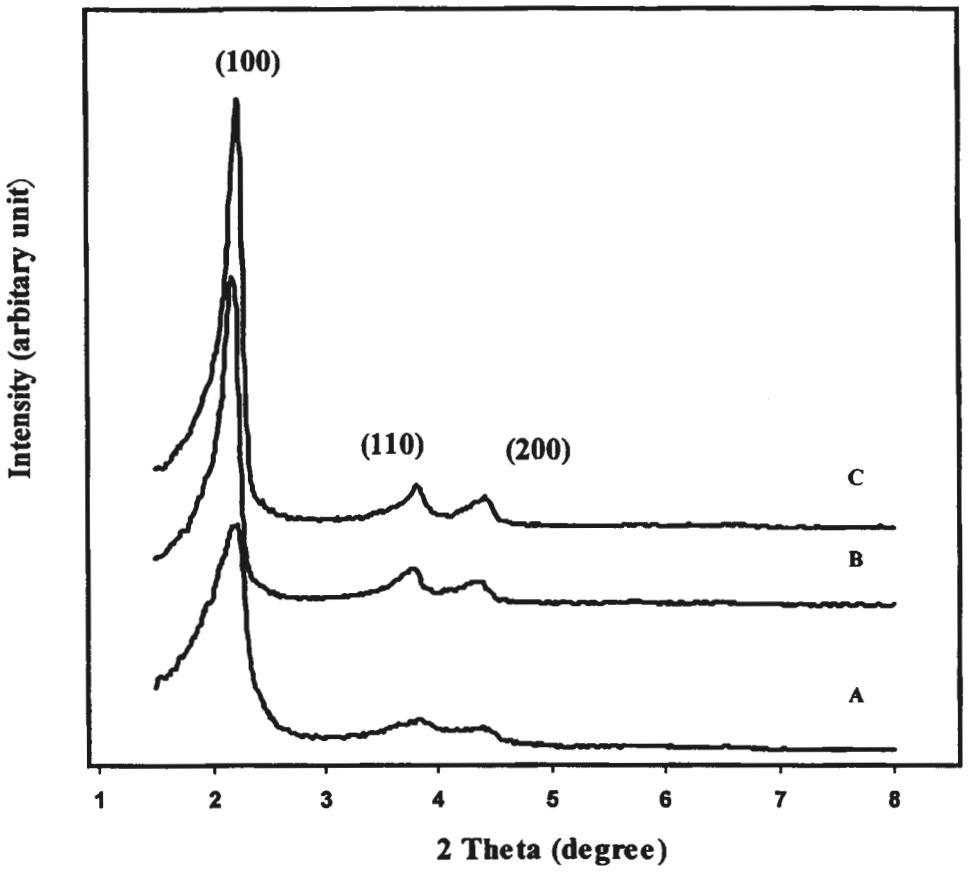

Figure 4.3 XRD patterns of calcined Sample CS-Na with different Si/Al ratios in catalyst: (A) 22.5; (B) 42.0; (C) 76.8.

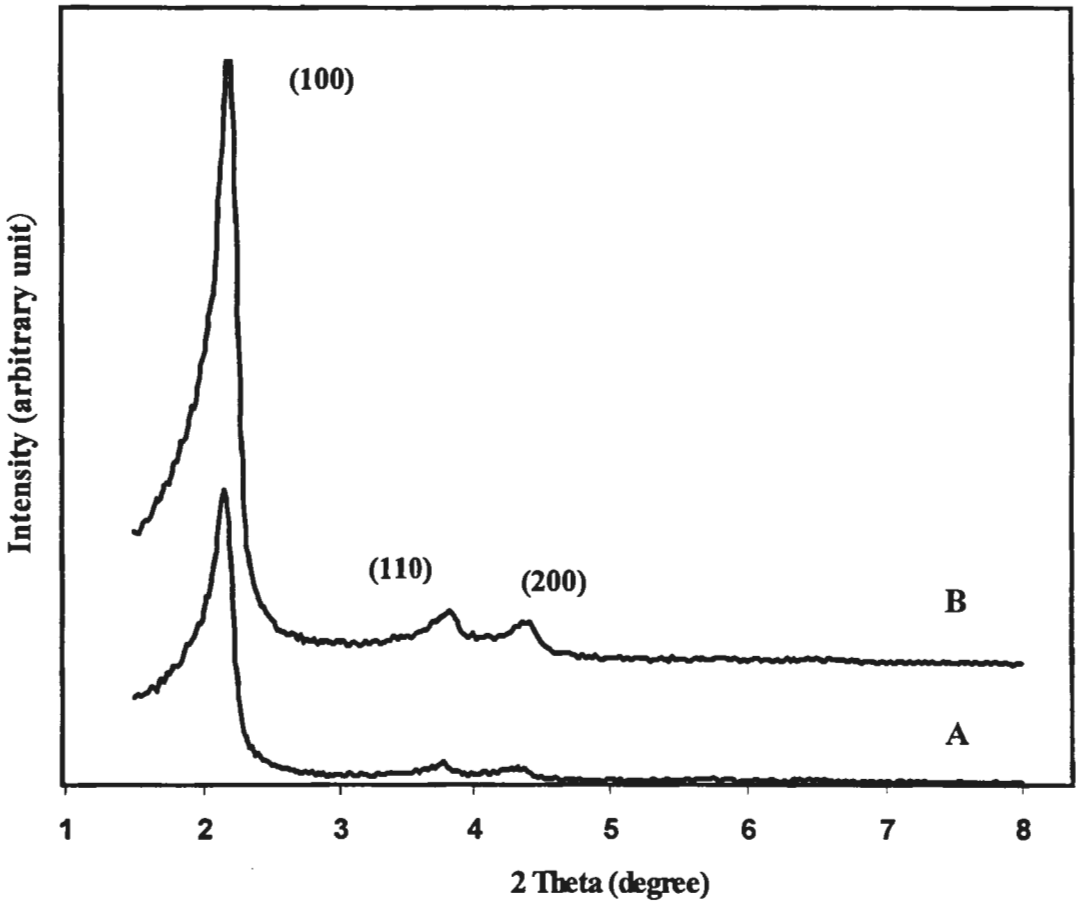

Figure 4.4 XRD patterns of CS-Na-20; (A) as-synthesized sample and (B) calcined sample.

4.2.3 SEM Images

SEM images shows of SS-20 and CS-Na-20 are shown in Figure 4.5. The particle shape of the former is spherical with 270 nm diameter, while the latter is coral-like with the size of 175 x 580 nm as shown in Figure 4.5 (A) and 4.5 (B), respectively. This indicates that the particle morphology is strongly affected by the type of silica source.

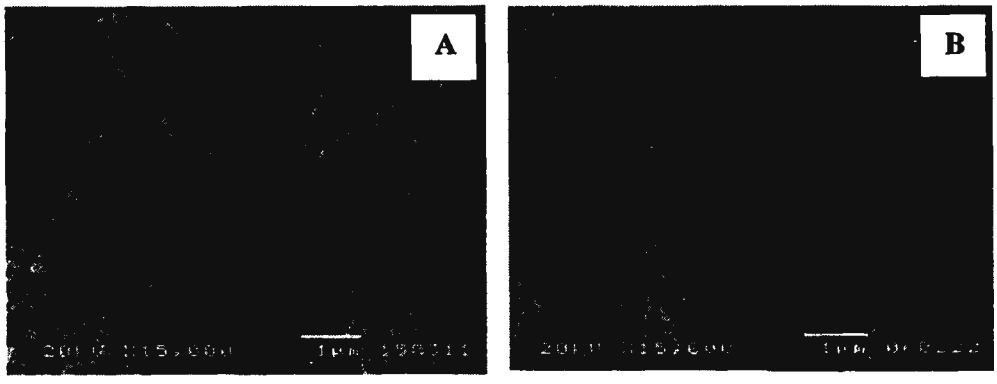

Figure 4.5 SEM images of calcined sample Al-MCM-41 with different SiO_2 sources: (A) Sample SS-20 and (B) Sample CS-Na-20.

4.2.4 ^{27}Al-MAS-NMR Spectra

Figure 4.6 and 4.7 shows the ^{27}Al-MAS-NMR spectra of as-synthesized and calcined Sample CS-Na with various Si/Al ratios. In Figure 4.6 the signal at 53 ppm is typically assigned to tetrahedrally coordinated (T_d) framework aluminum, and the peak at 0 ppm is assigned to the octahedrally coordinated (O_h) non-framework aluminum [81]. Only the signal of aluminum atoms at the framework site was observed for the as-synthesized samples. As aluminum content increased, the signals at the framework site increased in intensity. In Figure 4.7 the removal of the template by calcination led to the appearance of the signal at 0 ppm due to partial dealumination from the tetrahedral framework site. At low aluminum content (Si/Al=76.8) the ^{27}Al-MAS-NMR spectrum presents only the framework position. When aluminum content increased, the signals at both sites increased in intensity. However, the aluminum atoms preferably remain at tetrahedral framework position. The result indicates that aluminum migrates from tetrahedral sites to octahedral sites upon thermal treatment. This is in agreement with Kosslide *et al.* [82].

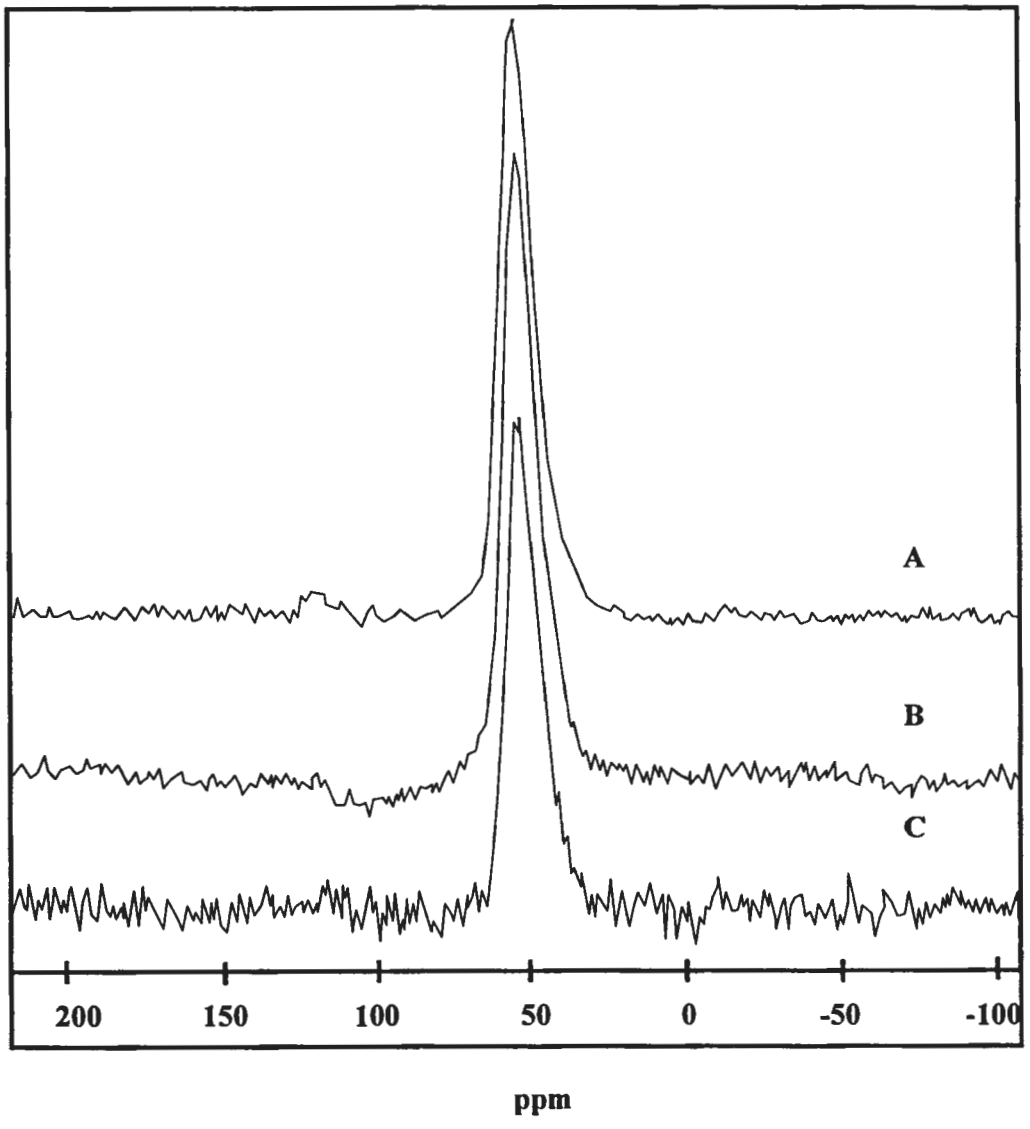

Figure 4.6 ^{27}Al-MAS-NMR spectra of as-synthesized Sample CS-Na with different Si/Al ratios in catalyst (A) 22.5; (B) 42.0; (C) 76.8.

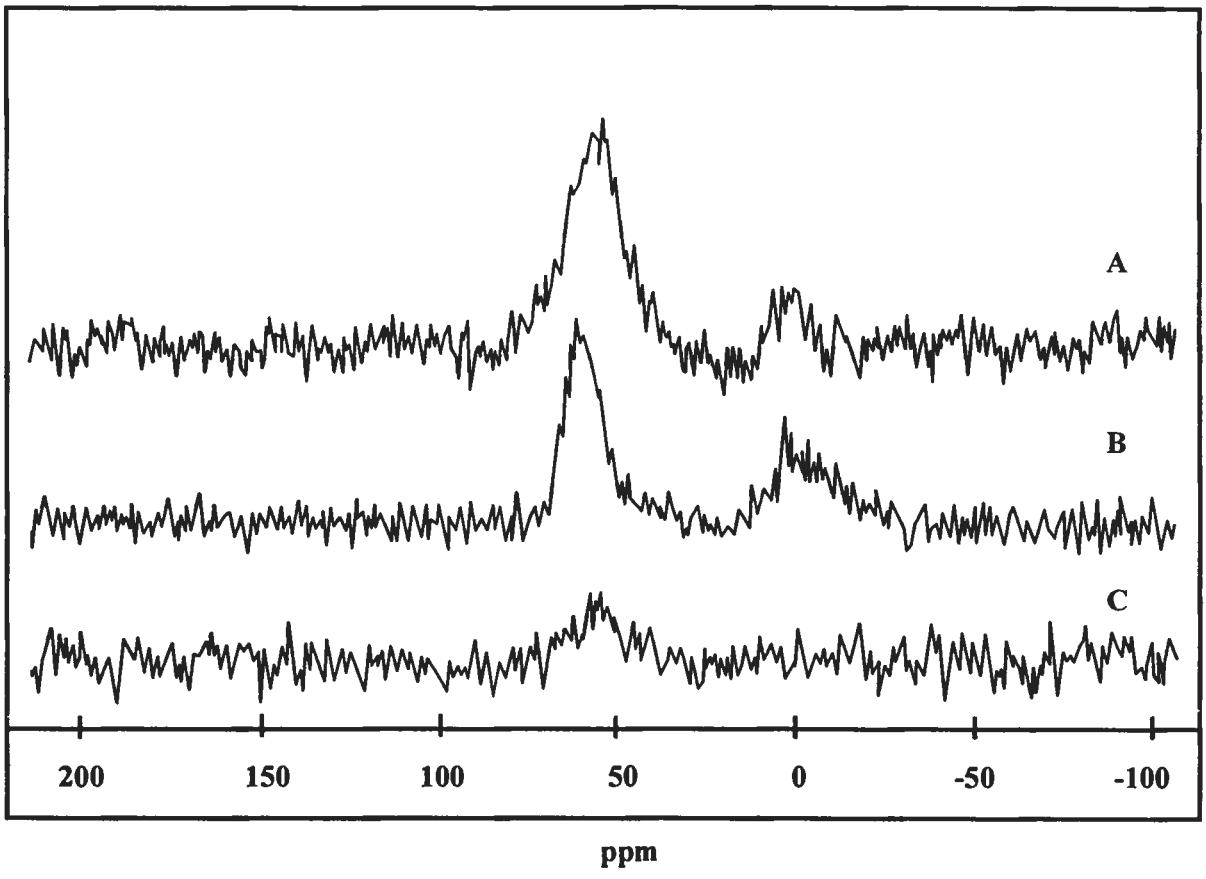

Figure 4.7 ^{27}Al-MAS-NMR spectra of Sample CS-Na with different Si/Al ratios in catalyst (A) 22.5; (B) 42.0; (C) 76.8.

4.2.5 Nitrogen Adsorption-Desorption

The N_2 adsorption-desorption isotherms for the calcined Sample CS-Na with various Si/Al ratios are shown in Figure 4.8. The samples exhibit a type IV isotherm which is typical for mesoporous materials. Each isotherm exhibits three stages as follows: Adsorption at low pressure (P/Po < 0.3) is accounted by a monolayer adsorption of nitrogen on the walls of the mesopores. As the relative pressure increases (P/Po = 0.3-0.5), the second stage rises steeply as characteristic of capillary condensation happening within mesopores. At higher relative pressure (P/Po > 0.5), the plateau region is due to fully pore filling followed by multilayer adsorption on the outer surface of the particles. Increasing the Si/Al ratio led to a reduction in the amount of nitrogen uptaken due to the decrease of mesoporous volume. Textural properties of calcined Al-MCM-41 samples are shown in Table 4.2. Pore size distribution was obtained from the adsorption data by means of the Barrett, Joyner

and Halenda (BJH) method as shown in Figure 4.9. The distribution of mesopores is quite narrow and similar for all samples. The pore size distribution peaks of the calcined Al-MCM-41 samples are centered at about 2.43 nm.

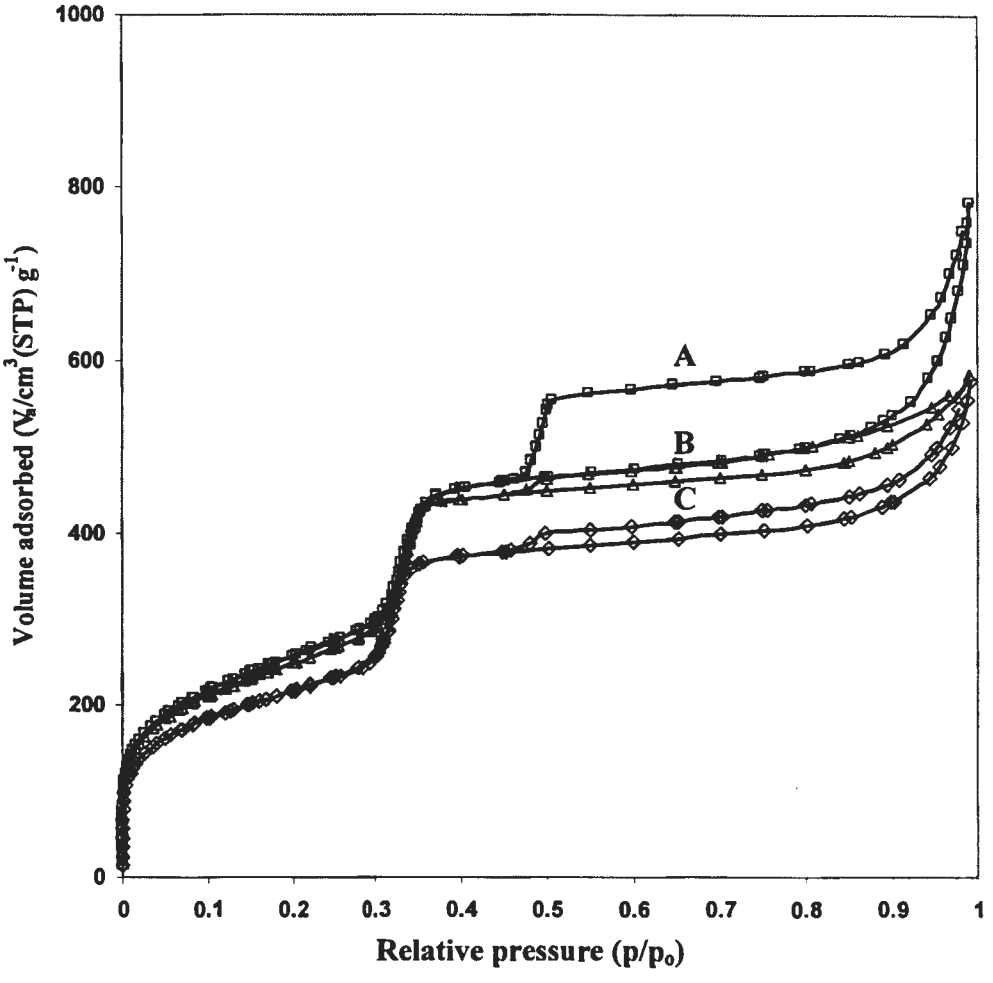

Figure 4.8 N_2 adsorption-desorption isotherms of Sample CS-Na with various Si/Al ratios in catalyst of (A) 22.5; (B) 40.0 and (C) 76.8.

Table 4.2 Textural properties of calcined Al-MCM-41 samples

Sample	d_{100} (nm.)	a_0 (nm.)[a]	S_{BET} (m^2/g)	d_p (nm.)	$V_{m\,(BET)}$ (cm^3(STP)/g)	Wall thickness (nm.)[b]
SS-20	4.13	4.77	750	2.43	173	2.34
CS-Na-20	4.00	4.62	928	2.43	212	2.19
CS-Na-40	4.02	4.64	894	2.43	206	2.21
CS-Na-80	4.17	4.81	795	2.43	183	2.38

a Hexagonal unit cell parameter calculated from $a_0 = 2d_{100} / \sqrt{3}$
b Wall-thicknesses calculated from a_0-d_p

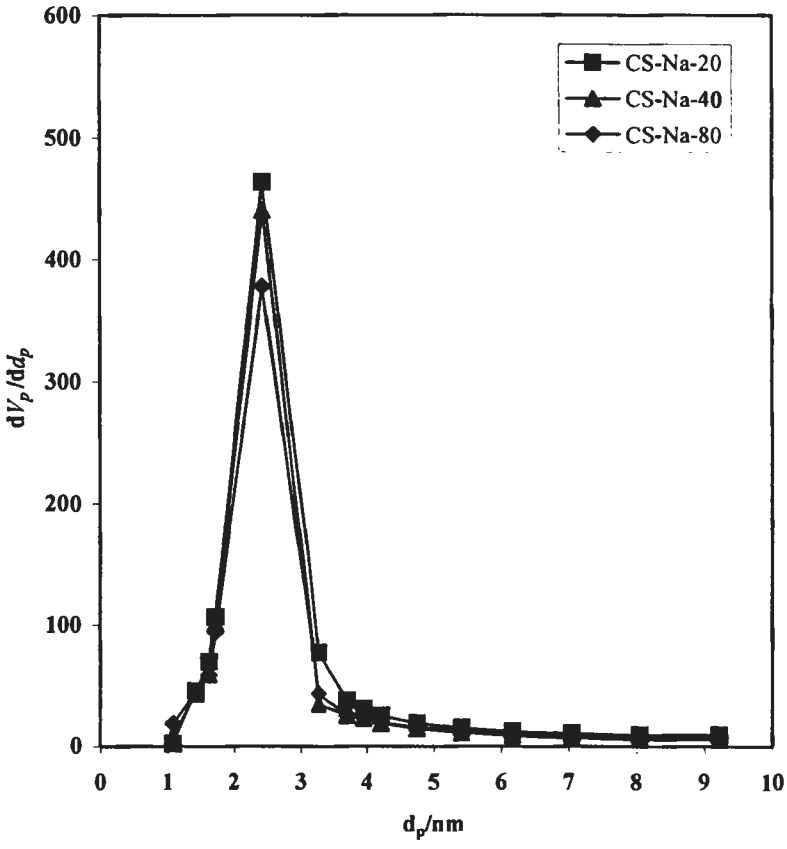

Figure 4.9 BJH pore-size distribution of Sample CS-Na with various Si/Al ratios in catalyst.

The model of pore structure for wall thickness calculation is depicted in Figure 4.10. The hexagonal unit cell parameter a_0 was calculated from the equation $a_0 = 2d_{100} / \sqrt{3}$. For Sample CS-Na, the d (100) value was increased from ca. 4.00 to 4.17 nm. , which indicates the increase in the lattice parameter. For a hexagonal structure, the wall thickness can be determined by the differences between the value of the unit cell (a_0) and pore diameter (d_p). The lower Al content, the thicker wall it has. Sample CS-Na-80 has the lowest specific surface area, smallest pore volume, and the thickest walls. Sample SS-20 and Sample CS-Na-80 show similar specific surface area and pore volume, but the latter material exhibits a slightly thicker wall. The thicker wall, the more thermal stability the sample has.

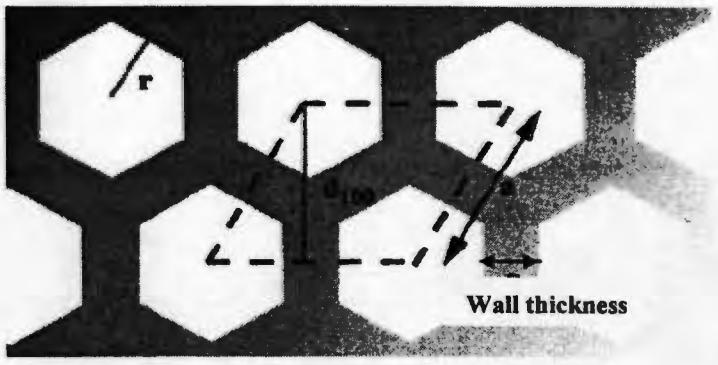

Figure 4.10 Schematic representation of the pore array of MCM-41. [83]

4.2.6 NH_3-TPD Profiles

Figure 4.11 shows NH_3-TPD profiles of Sample CS-Na-T with different Si/Al ratios. The NH_3-TPD profiles indicate that all samples exhibit two NH_3 desorption peaks corresponding to different acidity of the samples. The peak position corresponds to acid strength while the peak area corresponds to number of acid site. The peak centered at 150°C is typically assigned to a weaker acid site, and the other one at 350°C is assigned to a stronger acid site. It is obvious that the acid strength is similar for all three samples and only the number of acid sites is different. The number of weaker acid sites decreases when the Si/Al ratio increases due to the decrease in aluminum content in catalyst. The number of stronger acid site is pronounced for Sample CS-Na-20, and decrease for Sample CS-Na-40 and Sample CS-Na-80, respectively.

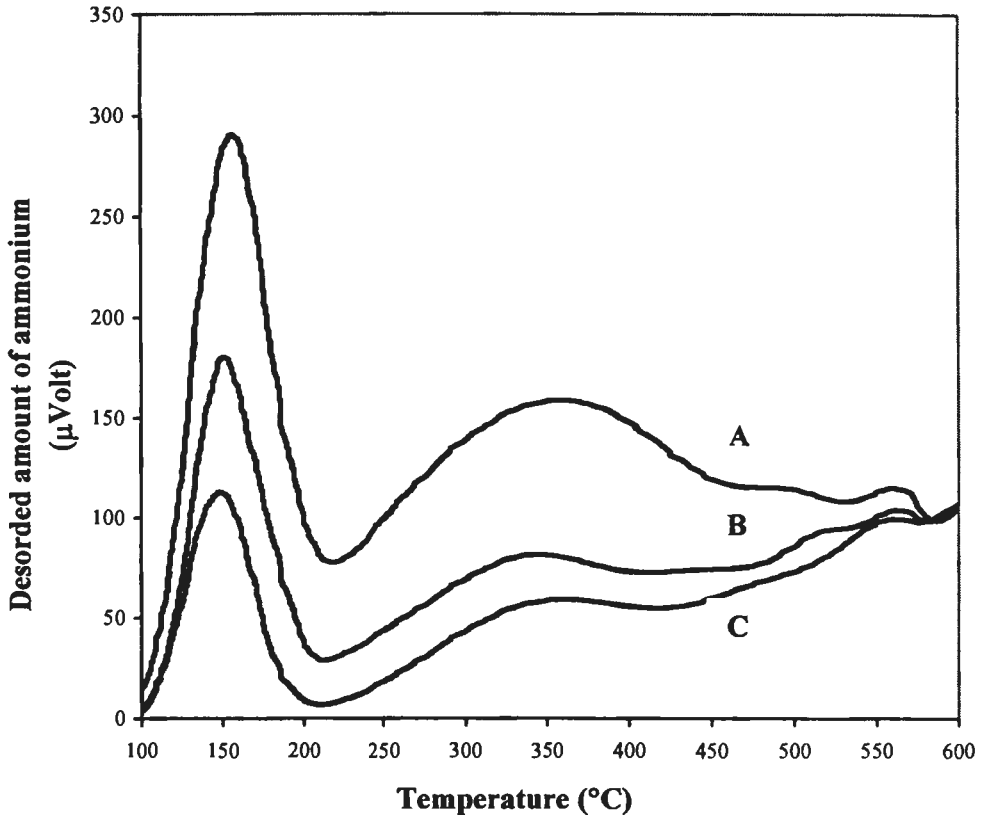

Figure 4.11 NH_3-TPD profiles of Sample CS-Na-T with various Si/Al ratios in catalyst (A) 22.5; (B) 40.0 and (C) 76.8.

4.3 The Optimal Condition for Ammonium Chloride Treatment of Sample CS-Na-20

4.3.1 Effect of Concentration of NH_4Cl Solution

^{27}Al-MAS-NMR spectra of the calcined Sample CS-Na-T-20 obtained by treating Sample CS-Na-20 with different NH_4Cl concentrations are shown in Figure 4.12. After thermal treatment to transform ammonium ions to protons which are the counter ions for negative framework charge due to $[AlO_2]^-$, relative intensities of tetrahedral Al to octahedral Al changes depending on the concentrations of NH_4Cl solution. Obviously, a part of octahedral non-framework aluminum migrates backward to the tetrahedral framework site during the ammonium ion treatment. If the NH_4Cl concentration is lower than 0.03 M, the sample, which is unstable to water,

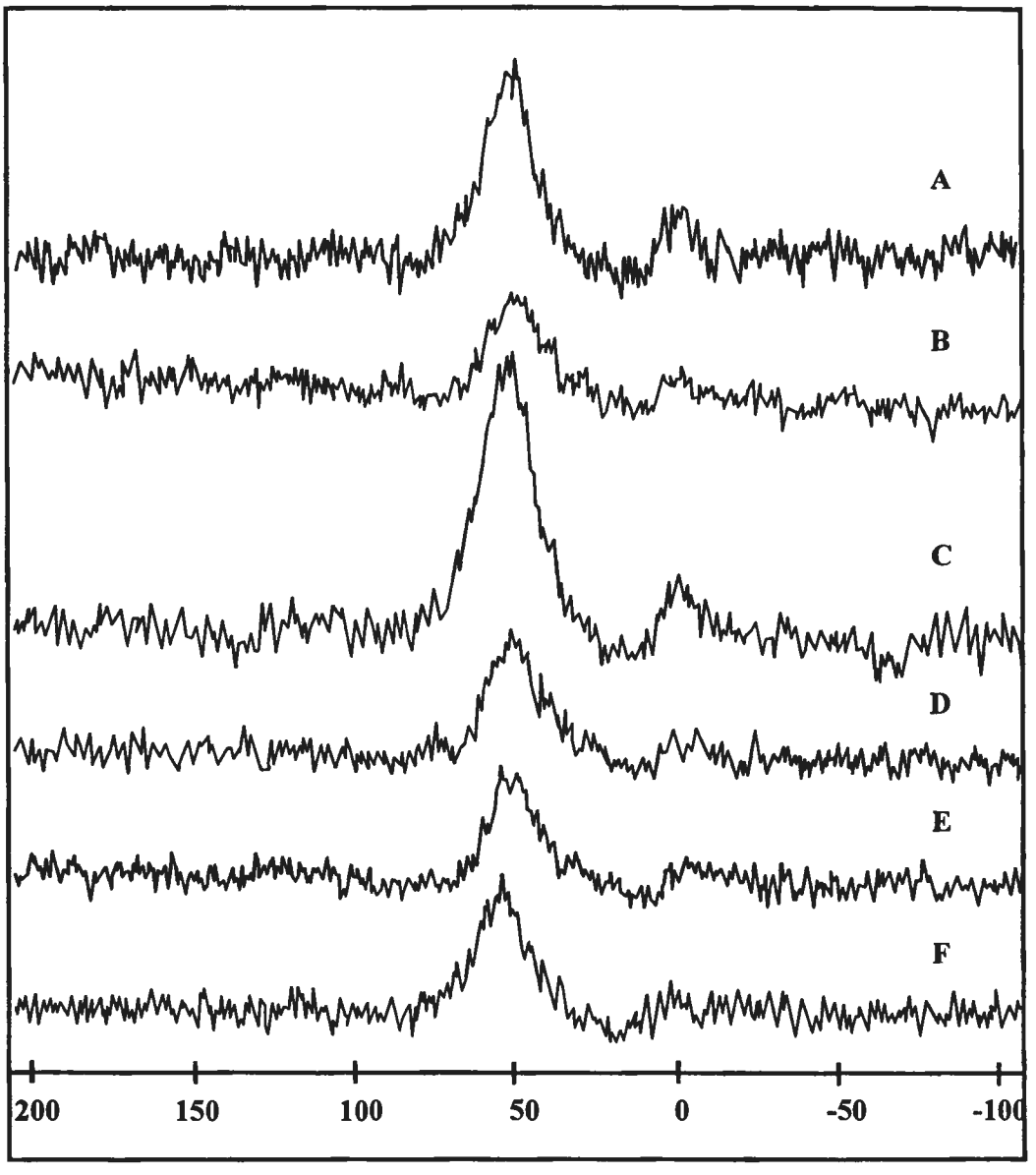

Figure 4.12 ^{27}Al-MAS-NMR spectra of (A) untreated Sample CS-Na-20 and Sample CS-Na-T-20 obtained by treating sample in NH_4Cl at different concentrations for 3 h: (B) 0.01 M; (C) 0.03 M; (D) 0.05 M; (E) 0.1 M; (F) 1 M.

tends to decompose causing Al leaching from solid to solution. If the NH_4Cl concentration is higher than 0.03 M, the considerable decrease of intensity was observed, especially for the tetrahedral framework Al peak. Only the NH_4Cl concentration of 0.03 M can increase the peak intensity of tetrahedral Al. The result was confirmed with repeated experimental. This indicates that the optimal condition for ammonium treatment is the utilization of 20 cm^3 0.03 M NH_4Cl solution for 1g catalyst to provide the highest relative intensity of tetrahedral Al to octahedral Al.

4.3.2 Effect of Reflux Duration

^{27}Al-MAS-NMR spectra of CS-Na-T-20 with different durations of ammonium treatment are shown in Figure 4.13. Considering the spectra in Figure 4.13, the peak intensity of tetrahedral Al seems to be not different, but in fact the relative intensity of tetrahedral Al to octahedral Al is quite different. It was found that one-hour treatment is not enough, while three- and six-hour treatment gave similar results of higher relative peak intensities of tetrahedral Al to octahedral Al. Then, the treatment with 0.03 M NH_4Cl solution for 3 h is selected to be the optimal condition and used for catalyst preparation for catalytic activity tests. Migration of Al from the tetrahedral site to octahedral Al site upon calculation of Al-MCM-41 and again backward from octahedral Al site to tetrahedral Al site after NH_4Cl treatment indicates the reversible migration process of Al. According to the result, the period of 3 h NH_4Cl treatment was selected for catalyst preparation for the rest of study in this work.

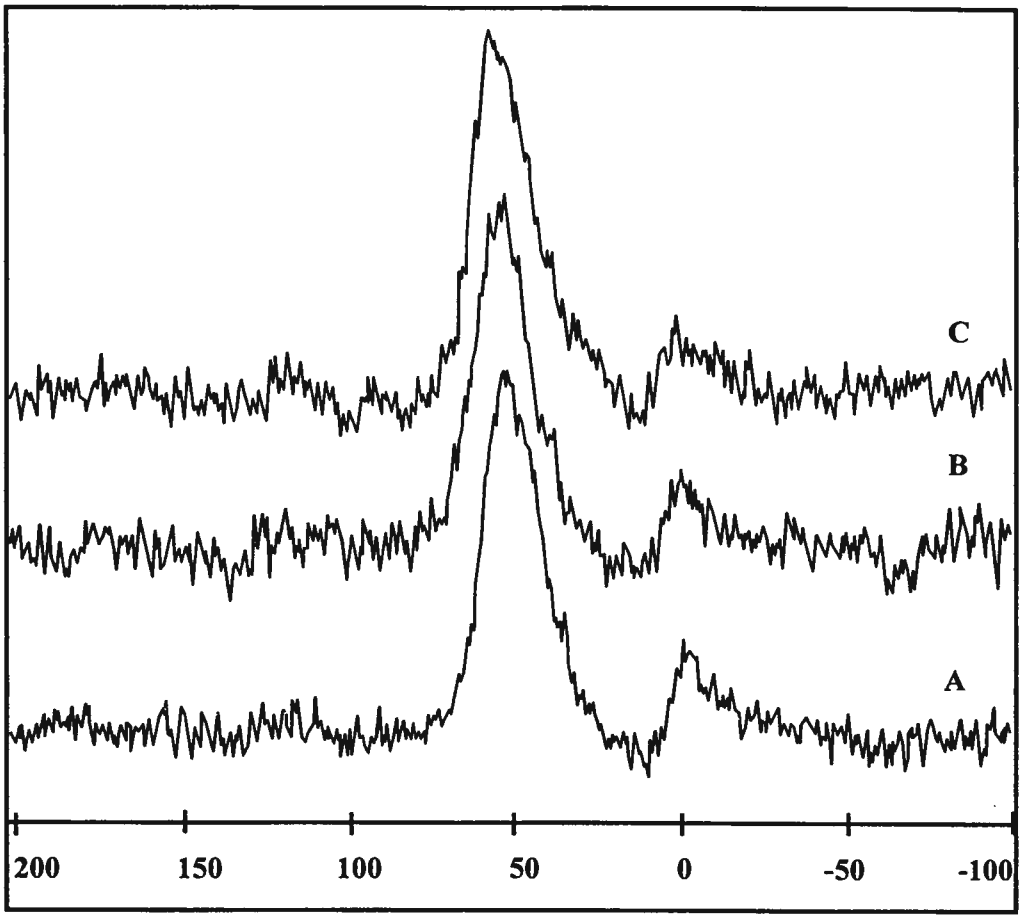

Figure 4.13 ^{27}Al-MAS-NMR spectra of Sample CS-Na-20 treated with 0.03M NH_4Cl for (A) 1 h; (B) 3 h; (C) 6 h.

4.4 Activity of Various Al-MCM-41 Catalysts in HDPE Cracking

4.4.1 Effect of Temperature

Sample CS-Na-T-20 was used for studying the effect of temperature on its activity. The thermal cracking in the absence of temperature was tested in comparison. The values of %conversion and the product yields for the thermal cracking and catalytic cracking of HDPE over Sample CS-Na-T-20 at 380°C and 400°C are shown in Table 4.3. The value of %conversion increases when reaction temperature increases from 380°C to 400°C. For thermal cracking at both reaction temperatures, no liquid fractions was found in the graduated cylinder. The result shows the difficulty in degradation of HDPE without catalyst at the temperature about 400°C or less. For such a case, the total weight loss of plastic precursor after reaction is devoted to gas fraction. The white candle wax remained in the reactor after the reaction was included in the residue. For the catalytic cracking, when the reaction temperature increases from 380°C to 400°C, the amount of residue decreases from 37.20 wt% to 5.70 wt%. The result indicated that the waxy residue decomposed into relatively lighter liquid hydrocarbons resulting in higher yield of liquid fractions than the case of thermal cracking. The liquid fractions have dark yellow color in both temperatures.

Table 4.3 Values of %conversion and %yield obtained by thermal cracking and catalytic cracking of HDPE over Sample CS-Na-T-20 at 380°C and 400°C (Condition: 10 wt% catalyst of plastic, N_2 flow of 20 cm^3/min and reaction of 30 min)

	Reaction temperature=380°C		Reaction temperature=400°C	
	Thermal	CS-Na-T-20	Thermal	CS-Na-T-20
%Conversion*	2.60	62.80	5.00	94.30
%Yield*				
1. gas fraction	2.60	26.10	5.00	31.70
2. liquid fraction	0.00	36.70	0.00	62.60
- % distillated oil	-	*51.06*	-	*59.99*
- % heavy oil	-	*48.94*	-	*40.01*
3. residue	97.40	37.20	95.00	5.70
- wax	*97.40*	*23.67*	*95.00*	*3.20*
- solid coke	-	*13.53*	-	*2.50*
Total volume of liquid fraction (cm^3)	-	2.55	-	4.25
Liquid fraction density (g/ cm^3)	-	0.7181	-	0.7365

*Deviation within 0.8% for conversion, 0.6% for yield of liquid fraction, and 0.8% for yield of residue.

Figure 4.14 shows the accumulative volume of liquid fractions in the graduated cylinder and the temperature of the reactor increased as a function of lapsed time. The initial rate of liquid fraction formation at 400°C is much faster than that at 380°C and higher total volume of liquid fraction was obtained for the 400°C compared to that at 380°C.

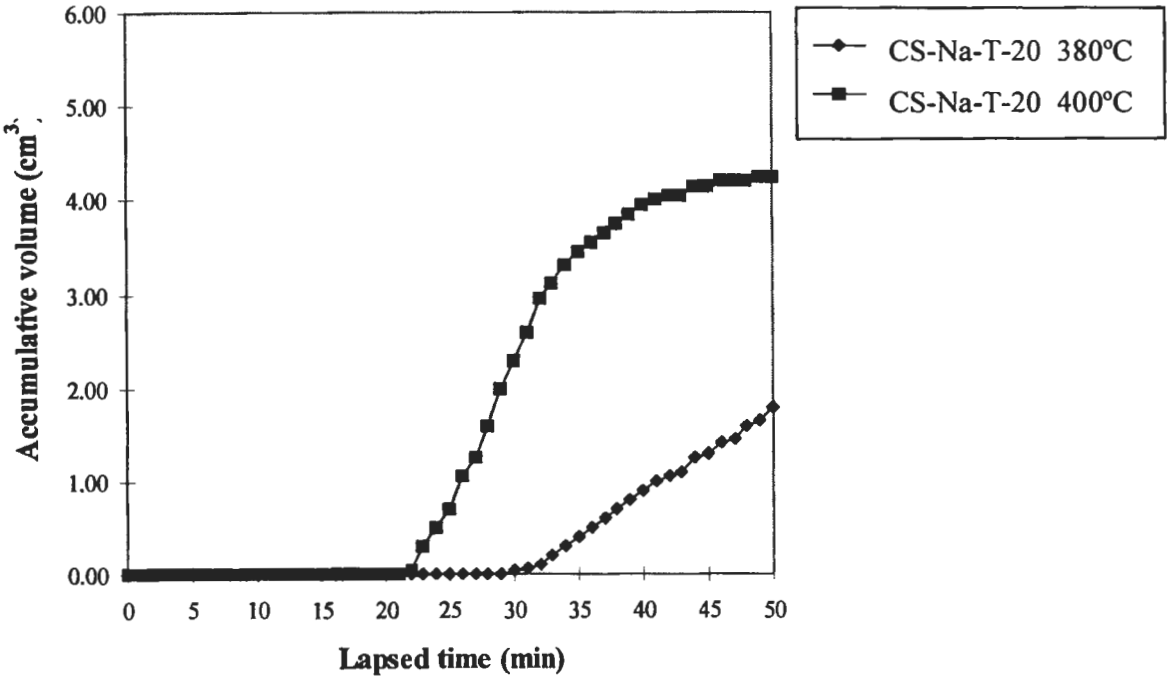

Figure 4.14 Accumulative volume of liquid fractions obtained by thermal cracking and catalytic cracking of HDPE over Sample CS-Na-T-20 at 380°C and 400°C (Condition: 10 wt% catalyst of plastic, N_2 flow of 20 cm^3/min and reaction of 30 min).

Figure 4.15 shows distribution of gas fraction obtained by thermal cracking and catalytic cracking of HDPE over Sample CS-Na-T-20 at 380°C and 400°C. Considering only gases at ambient condition which are normally C_1 through C_5, the major component for thermal cracking is C_4 (n-butane) while that for catalytic cracking is C_3 (propene) independently from temperature. However, the vapor of C_5^+

(liquids at ambient condition) which has higher boiling point than that of C_5 (n-pentane) is obviously detected in a significant amount.

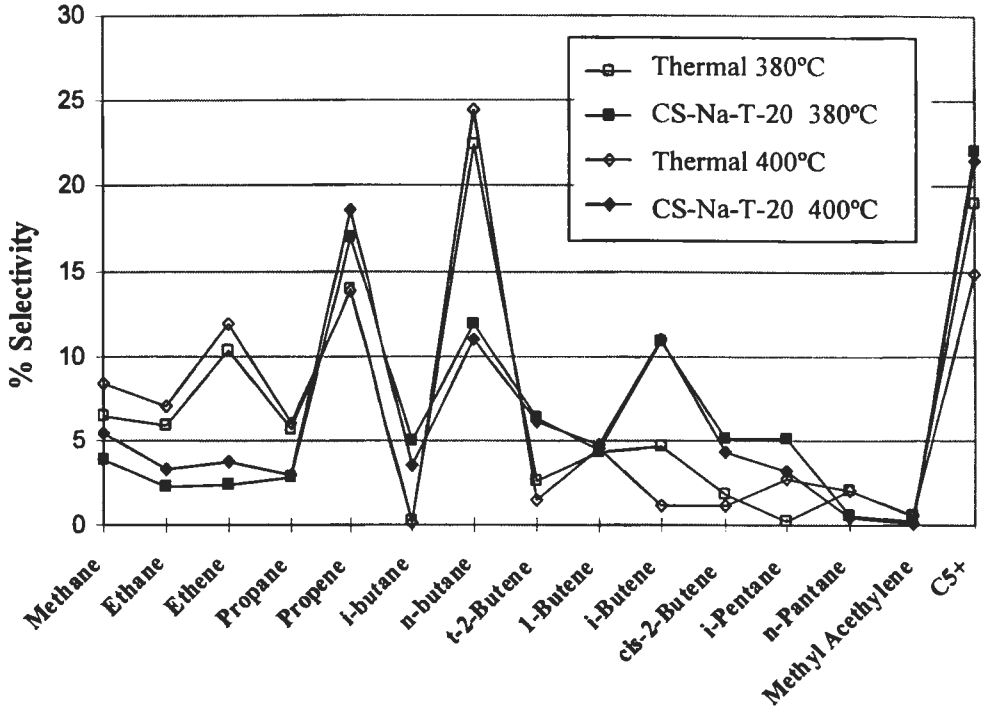

Figure 4.15 Distribution of gas fraction obtained by the thermal cracking and catalytic cracking of HDPE over Sample CS-Na-T-20 at 380°C and 400°C (Condition: 10 wt% catalyst of plastic, N_2 flow of 20 cm^3/min and reaction of 30 min).

Figure 4.16 shows product distribution of distillate oil obtained by thermal cracking and catalytic cracking of HDPE over Sample CS-Na-T-20 at 380°C and 400°C. The distillate oil components are mainly in the range of C_7 to C_8. When the reaction temperature increases, the liquid fractions of lighter hydrocarbon (C_5-C_6) increases while that of heavier hydrocarbon (C_8-C_9) decreases. However, this change is not significant. According to the results of temperature effect on HDPE cracking, the temperature of 400°C is selected to be the test condition for further studies in this work due to considerably large amount of liquid fractions was obtained.

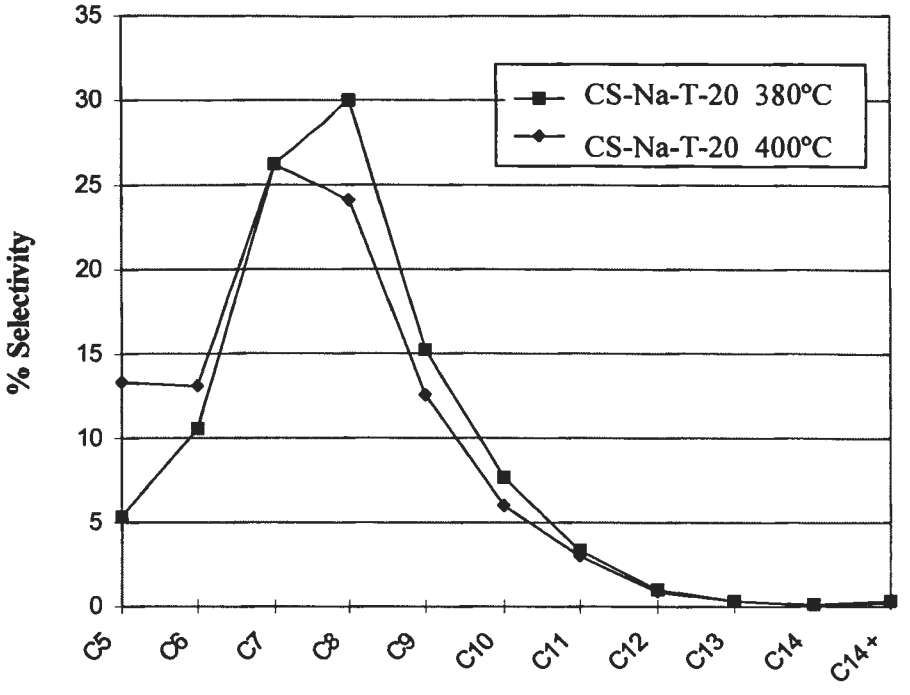

Figure 4.16 Carbon number distribution of liquid fractions from catalytic cracking of HDPE over Sample CS-Na-T-20 at 380°C and 400°C (Condition: 10 wt% catalyst of plastic, N_2 flow of 20 cm^3/min and reaction of 30 min).

4.4.2 Effect of Si/Al Ratios in Catalyst

The values of %conversion and product yield obtained by the catalytic cracking of HDPE over Sample CS-Na and Sample CS-Na-T catalysts with different Si/Al ratios at 400°C are compared in Table 4.4. With higher Si/Al ratios above 20 the catalysts perform higher %conversion after they were treated with NH_4Cl. This is due to the removal of trace amount of Na^+ ions, behaving as cations balancing together with the main $CTMA^+$ cations the framework charges, by NH_4Cl treatment. Considering the catalyst with Si/Al ratio of 20, relatively high aluminum content, there is no difference in %conversion between the activities of NH_4Cl treated and untreated catalysts. This means such as effect is not pronounced for the case of high aluminum content or high acidity. The impact is more significant on the yields of liquid fraction and gas fraction. All NH_4Cl treated catalysts provide more liquid fraction yield and less gas fraction yield than the untreated catalysts. Nevertheless, the distillated oil was produced in larger amount than heavy oil and much less coke was formed after the NH_4Cl treatment of all three catalysts. All liquid fractions have dark yellow color. The color of treated sample is bright than those untreated sample.

Table 4.4 Values of %conversion and %yield obtained by catalytic cracking of HDPE over Sample CS-Na and Sample CS-Na-T catalysts with various Si/Al ratios (Condition: 10 wt% catalyst of plastic, N_2 flow of 20 cm^3/min, 400°C, and reaction time of 30 min)

	CS-Na-20	CS-Na-40	CS-Na-80	CS-Na-T-20	CS-Na-T-40	CS-Na-T-80
%Conversion*	94.30	89.90	89.09	94.30	93.21	92.52
%Yield*						
1. gas fraction	40.80	36.30	35.64	31.70	33.57	33.93
2. liquid fraction	53.50	53.60	53.45	62.60	59.64	58.59
- % distillated oil	*52.54*	*49.15*	*51.93*	*59.99*	*56.95*	*56.06*
- % heavy oil	*47.46*	*50.85*	*48.07*	*40.01*	*43.05*	*43.94*
3. residue	5.70	10.10	10.91	5.70	6.79	7.48
- wax	*1.40*	*7.60*	*9.62*	*3.20*	*5.92*	*7.02*
- solid coke	*4.30*	*2.50*	*1.29*	*2.50*	*0.87*	*0.46*
Total volume of liquid fraction (cm^3)	3.68	3.68	3.63	4.25	4.05	3.85
Liquid fraction density (g/ cm^3)	0.7279	0.7293	0.7366	0.7365	0.7371	0.7623

*Deviation within 0.4% for conversion, 0.8% for yield of liquid fraction, and 0.4% for yield of residue.

Considering data in Table 4.4 for untreated calcined Sample CS-Na catalysts, the decrease of Si/Al ratio from 20 to 40 led to less conversion but there is no difference in conversion for Sample CS-Na-40 and Sample CS-Na-80. The specific surface area cannot explain the activity of those catalysts because their activities do not relate to the change in specific surface area. The number of active site, determined by NH_3-TPD method, is accounted for their behavior as discussed previously in Section 4.2.6. Both Sample CS-Na-80 and Sample CS-Na-40 have not different in term of number of acid sites; therefore, their activities are not different. NH_3-TPD of untreated calcined Sample CS-Na catalysts was not measured. In the reaction, the catalyst need NH_4Cl treatment for decreased the cations on surface. For NH_4Cl treatment Sample CS-Na catalysts, the conversion for CS-Na-T samples decrease as Si/Al ratio increases. This is in agreement with the decrease in acidity of these catalysts as previously mentioned in Section 4.2.6.

The liquid fraction yields are about the same for Sample CS-Na-20, Sample CS-Na-40, and Sample CS-Na-80 catalysts. The gas fraction yield and the

residue portion for Sample CS-Na-20 are different from those for untreated catalysts. From Sample CS-Na-20 to Sample CS-Na-40, the yield of gas fraction decreases while that of residue portion increases. The reason is the effect of acidity as accounted for conversion. The higher actual acidity, determined by NH_3-TPD method, causes higher efficiency in cracking HDPE to products and less residue was left in the catalytic reactor. Similarly, the performance of Sample CS-Na-T catalysts is also described by the actual acidity of the catalyst.

Figure 4.17 shows the accumulated volume of liquid fraction obtained by catalytic cracking of HDPE over various Al-MCM-41 catalysts at 400°C along the lapsed time spent since heating started. The increase in rate of liquid fraction formation was observed after the NH_4Cl treatment of all three catalysts with different Si/Al ratios. Although the initial rates of liquid fraction formation for Sample CS-Na-20 and Sample CS-Na-T-20 are not different but the overall rates of liquid fraction formation over Sample CS-Na-T-20 is faster than that over Sample CS-Na-20. The effect of the NH_4Cl treatment is more pronounced for the catalysts with Si/Al ratios of 40 and 80.

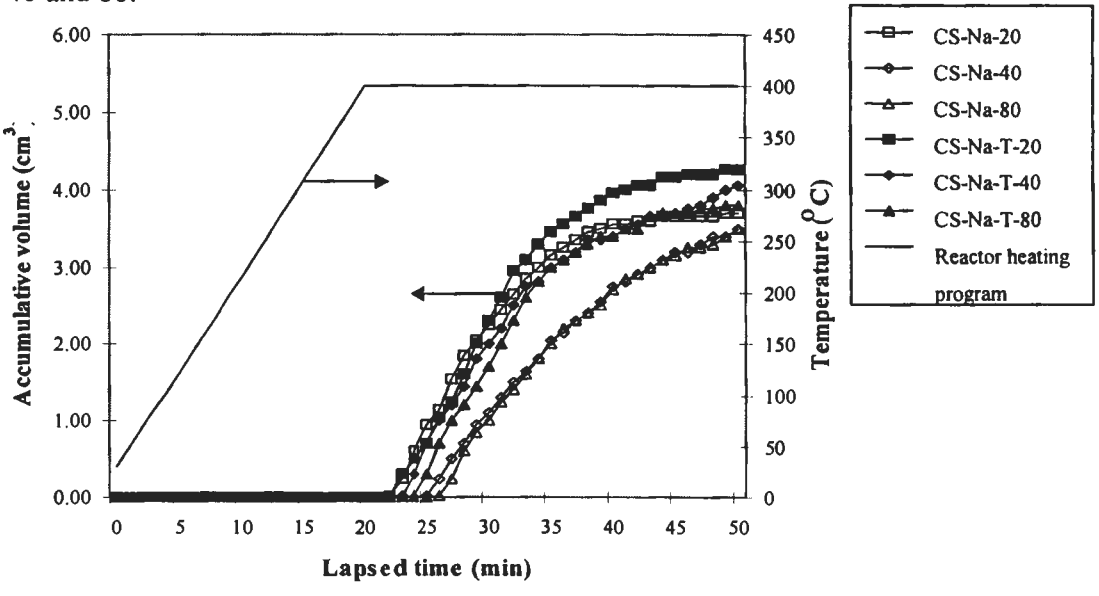

Figure 4.17 Accumulative volume of liquid fractions from catalytic cracking of HDPE over various Al-MCM-41 catalysts at 400°C (Condition: 10 wt% catalyst of plastic, N_2 flow of 20 cm^3/min and reaction of 30 min).

Figure 4.18 shows distribution of gas fraction obtained by catalytic cracking of HDPE over various Al-MCM-41 catalysts at 400°C. In the presence of any Al-MCM-41 catalysts, the product distribution in gas fraction is different from that in the absence of catalyst or thermal pyrolysis. The major component is propene for the catalytic cracking while it is n-butane for thermal pyrolysis. The product distribution in gas fraction is independent from the NH_4Cl treatment of the catalysts and the Si/Al ratio in the catalyst.

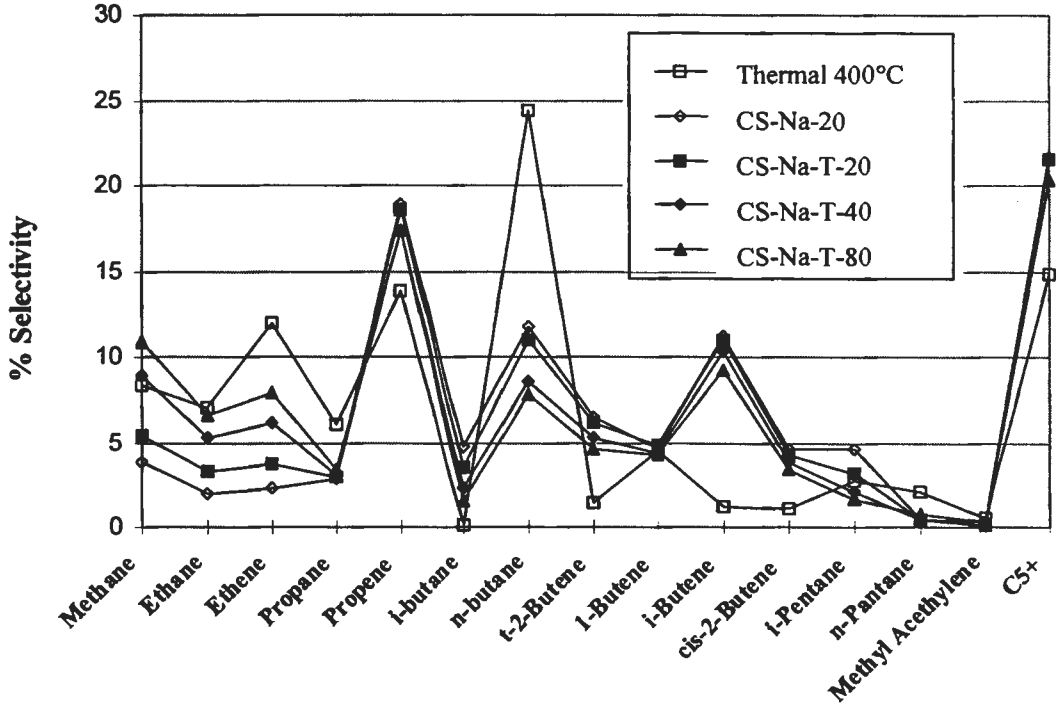

Figure 4.18 Distribution of gas fraction obtained by catalytic cracking of HDPE over various Al-MCM-41 catalysts at 400°C (Condition: 10 wt% catalyst of plastic, N_2 flow of 20 cm^3/min and reaction of 30 min).

Figure 4.19 shows product distribution of distillated oil obtained by catalytic cracking of HDPE from catalytic cracking of HDPE over various Al-MCM-41 catalysts at 400°C. Obviously, the product distribution in liquid phase is affected by both the NH_4Cl treatment of the catalysts and the Si/Al ratio in catalyst. The major products are distributed in the range of C_7 and C_8 increases as the Si/Al ratio increases. Surprisingly, the NH_4Cl treatment of Sample CS-Na-20 causes the decrease of the selectivity to C_7 and C_8 components. The product distribution of SUPELCO

standard gasoline fraction is shown in Figure 4.20. The major components are C_7 and C_8. That is comparable to the distribution of distillate oil obtained in this work based on the boiling point range using n-paraffins as reference.

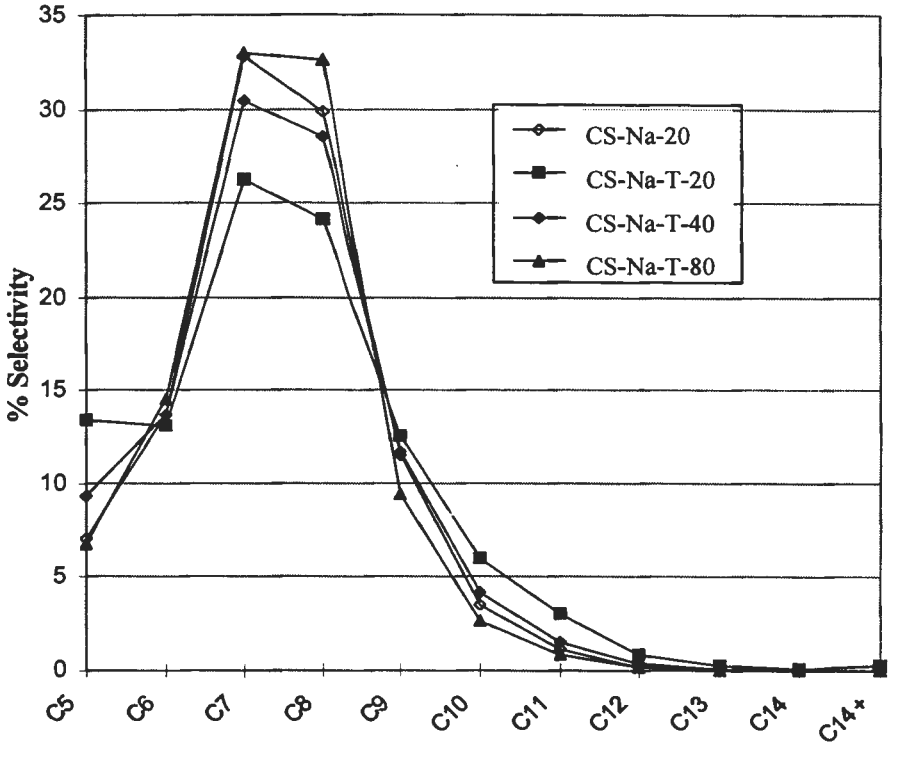

Figure 4.19 Carbon number distribution of distillated oil obtained by catalytic cracking of HDPE over various Al-MCM-41 catalysts at 400°C (Condition: 10 wt% catalyst of plastic, N_2 flow of 20 cm^3/min and reaction of 30 min).

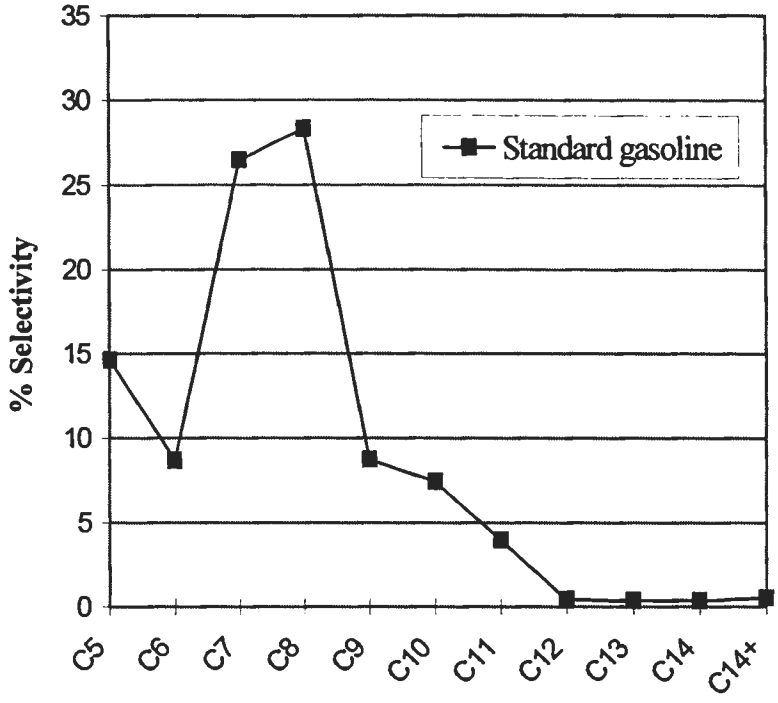

Figure 4.20 Carbon number distribution of commercial SUPELCO standard gasoline fraction.

4.5 Activity of Various Al-MCM-41 Catalysts in PP Cracking

4.5.1 Effect of Temperature

Table 4.5 shows the values of %conversion and %yield obtained by the thermal cracking and catalytic cracking of PP over Sample CS-Na-T-20 at 380°C and 400°C. The PP cracking takes place more easily than the HDPE cracking due to the more stability of carbonium and carbenium ions originated from PP than that from HDPE during the cracking process. Increasing temperature from 380°C and 400°C resulted in much higher conversion of PP by thermal cracking. For the cracking at 380°C in the presence of Sample CS-Na-T-20, the conversion of PP greatly increases compared to non-catalytic cracking. The activity of Sample CS-Na-T-20 is not affected at all by increasing temperature from 380°C to 400°C. That indicates the powerful catalyst Sample CS-Na-T-20 even at the temperature as low as 380°C. At both temperatures, the liquid fraction yields are considerable for the catalytic cracking compared to the thermal cracking. All liquid fractions have pale yellow color.

Table 4.5 Values of %conversion and %yield obtained by thermal cracking and catalytic cracking of PP at 380°C and 400°C (Condition: 10%wt catalyst of plastic, N_2 flow of 20 cm^3/min and reaction of 30 min)

	Reaction temperature=380°C		Reaction temperature=400°C	
	Thermal	CS-Na-T-20	Thermal	CS-Na-T-20
%Conversion*	28.20	95.40	75.40	95.60
%Yield*				
1. gas fraction	14.20	22.40	26.20	23.50
2. liquid fraction	14.00	73.00	49.20	72.10
- % distillated oil	*71.23*	*59.88*	*66.67*	*59.88*
- % heavy oil	*28.77*	*40.12*	*33.33*	*40.12*
3. residue	71.80	4.60	24.60	4.40
- wax	*71.80*	*2.25*	*24.60*	*2.05*
- solid coke	-	*2.35*	-	*2.35*
Total volume of liquid fraction (cm^3)	0.95	4.95	2.85	4.95
Liquid fraction density (g/ cm^3)	0.7368	0.7374	0.7569	0.7283

*Deviation within 0.2% for conversion, 0.2% for yield of liquid fraction, and 0.2% for yield of residue.

Figure 4.21 shows the volume of liquid fraction accumulated in the graduated cylinder and the temperature in the reactor as a function of lapsed time. The initial rate of 400°C is much faster than 380°C for both thermal cracking and catalytic cracking but the overall rates of liquid fraction formation are the same. That is due to the temperature dependence of kinetic effect. Thus on the purpose of conversion of plastic to liquid fuel, the temperature of 400°C was selected for the rest of work on the catalytic cracking of HDPE.

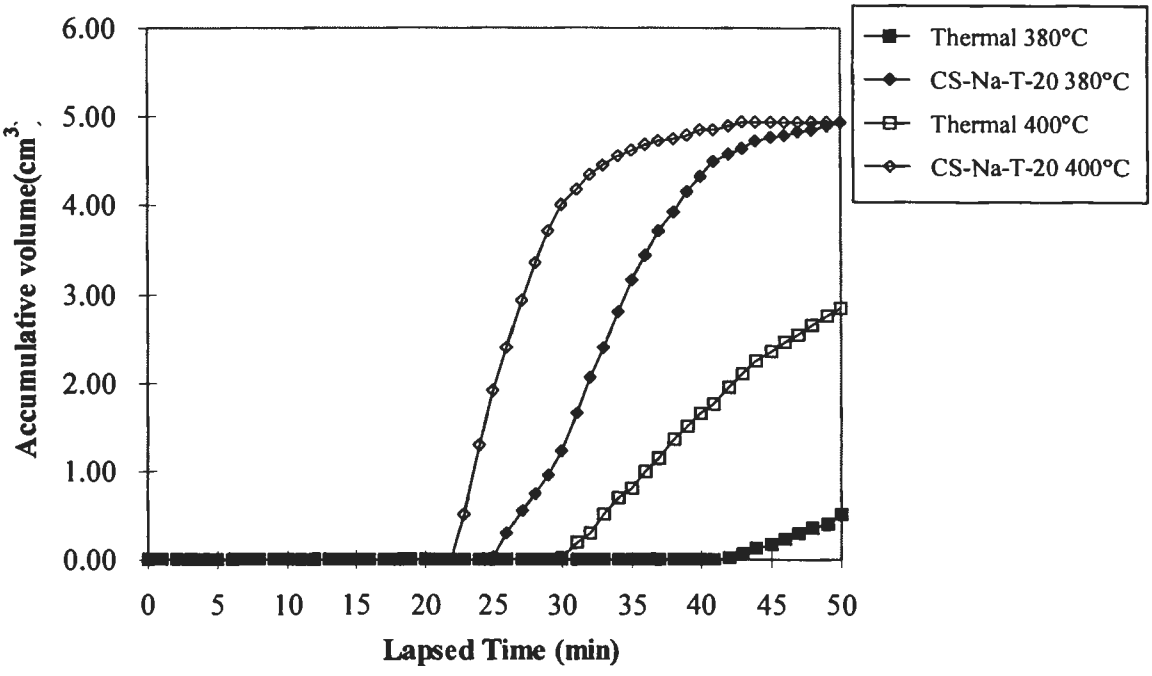

Figure 4.21 Accumulative volume of liquid fraction from thermal cracking and catalytic cracking of PP over Sample CS-Na-T-20 at 380°C and 400°C (Condition: 10 wt% catalyst of plastic, N_2 flow of 20 cm^3/min and reaction of 30 min).

Figure 4.22 shows distribution of gas fraction obtained by thermal cracking and catalytic cracking of PP over Sample CS-Na-T-20 at 380°C and 400°C. In thermal cracking, the distribution in gas fraction is mainly propene, n-butane and n-pentane. In catalytic cracking, the selectivity to i-butene increases and those to propene and n-pentane decrease.

Figure 4.23 shows product distribution of the liquid fraction obtained by thermal cracking and catalytic cracking of PP using Al-MCM-41 with the Si/Al of 20 at 380°C and 400°C. For the thermal cracking, the liquid fraction is mainly C_9 components. For the catalyst cracking at 380°C, the liquid fraction is mainly C_8 components. Catalyst cracking at 400°C, the liquid fraction is mainly C_7 components. When the temperature increases, the amount of lighter hydrocarbon in range of C_6- C_7 little increases while that of heavier hydrocarbon in range of C_8- C_9 little decreases.

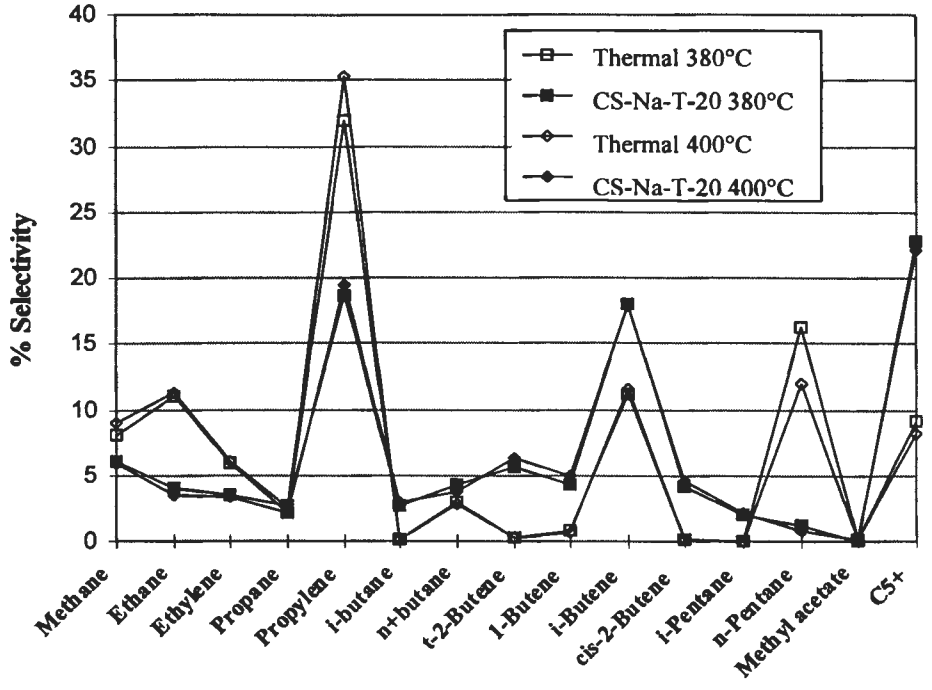

Figure 4.22 Distribution of gas fraction obtained by the thermal cracking and catalytic cracking of PP over Sample CS-Na-T-20 at 380°C and 400°C (Condition: 10 wt% catalyst of plastic, N_2 flow of 20 cm^3/min and reaction of 30 min).

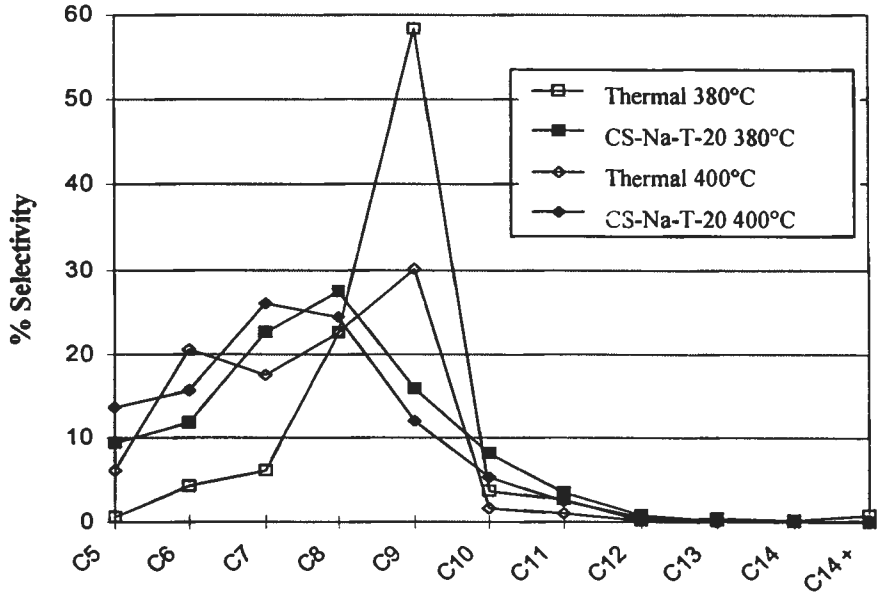

Figure 4.23 Carbon number distribution of liquid fraction obtained by catalytic cracking of PP over Sample CS-Na-T-20 at 380°C and 400°C (Condition: 10 wt% catalyst of plastic, N_2 flow of 20 cm^3/min and reaction of 30 min).

4.5.2 Effect of Si/Al Ratios in Catalyst

The values of %conversion and %yield obtained by the thermal cracking and catalytic cracking of PP over Sample CS-Na-T-20 catalysts with various Si/Al ratios at 380°C and 400°C are shown in Table 4.6 and Table 4.7, respectively. The %conversion for thermal cracking is lower than catalytic cracking. Catalytic cracking of Al-MCM-41, the yield of liquid fraction was higher and that of gas fraction was lower than those from thermal cracking. The %conversion and %yield are not significantly affected by the change in Si/Al ratio of the Al-MCM-41 catalyst at both temperatures. Considering data in Table 4.7, for non-acidic Si-MCM-41, the yield of products did not differ much from that of thermal cracking. This result also indicates that the solid acid catalyst promotes the degradation of the melt polymer into molecular weight compounds. All liquid fractions have pale yellow color.

Table 4.6 Values of %conversion and %yield obtained by thermal cracking and catalytic cracking of PP over Sample CS-Na-T-20 with various Si/Al ratios at 380°C (Condition: 10 wt% catalyst of plastic, N_2 flow of 20 cm^3/min and reaction of 30 min)

	Thermal	CS-Na-T-20	CS-Na-T-40	CS-Na-T-80
%Conversion*	28.20	95.40	95.30	95.20
%Yield*				
1. gas fraction	14.20	22.40	22.60	22.90
2. liquid fraction	14.00	73.00	72.70	72.30
- % distillated oil	71.23	*59.88*	*65.67*	*67.28*
- % heavy oil	28.77	*40.12*	*34.23*	*32.72*
3. residue	71.80	4.60	4.70	4.80
- wax	*71.80*	*2.25*	*3.12*	*3.38*
- solid coke	-	*2.35*	*1.58*	*1.42*
Total volume of liquid fraction (cm^3)	0.95	4.95	4.87	4.85
Liquid fraction density (g/ cm^3)	0.7368	0.7374	0.7457	0.7454

*Deviation within 0.2% for conversion, 0.4% for yield of liquid fraction, and 0.2% for yield of residue.

Table 4.7 Values of %conversion and %yield obtained by thermal cracking and catalytic cracking of PP over Sample CS-Na-T-20 with various Si/Al ratios at 400°C (Condition: 10 wt% catalyst of plastic, N_2 flow of 20 cm^3/min and reaction of 30 min)

	Thermal	Si-MCM-41	CS-Na-T-20	CS-Na-T-40	CS-Na-T-80
%Conversion*	75.40	85.20	95.60	95.50	95.40
%Yield*					
1. gas fraction	26.20	35.20	23.50	23.20	23.90
2. liquid fraction	49.20	50.00	72.10	72.30	71.50
- % distillated oil	66.67	*69.09*	*59.88*	*67.71*	*70.30*
- % heavy oil	33.33	*30.91*	*40.12*	*32.29*	*29.70*
3. residue	24.60	14.80	4.40	4.50	4.60
- wax	*24.60*	*12.20*	*2.05*	*2.57*	*2.47*
- solid coke	-	*2.60*	*2.35*	*1.93*	*2.13*
Total volume of liquid fraction (cm^3)	2.85	3.00	4.95	4.92	4.85
Liquid fraction density (g/ cm^3)	0.7569	0.7813	0.7283	0.7340	0.7371

*Deviation within 0.8% for conversion, 0.6% for yield of liquid fraction, and 0.8% for yield of residue.

Figure 4.24 shows accumulative volume of liquid fraction in the graduated cylinder. The initial rate of catalytic cracking is much faster than thermal cracking. The highest initial rate was Al-MCM-41 ratio of 20.

Figure 4.25 shows accumulative volume of liquid fraction in the graduated cylinder. The rate of liquid fraction formation for PP cracking over non-acidic Si-MCM-41, analogous to acidic Al-MCM-41, is not different from the thermal cracking in the absence of catalyst The rates of liquid fraction formation over Sample CS-Na-T catalysts with different Si/Al ratios are not much different but all are quite faster than both thermal cracking and that over non-acidic Si-MCM-41. That confirms the acidity effect of aluminum incorporated in the MCM-41 structure can play important role on activity of the catalysts in cracking of PP.

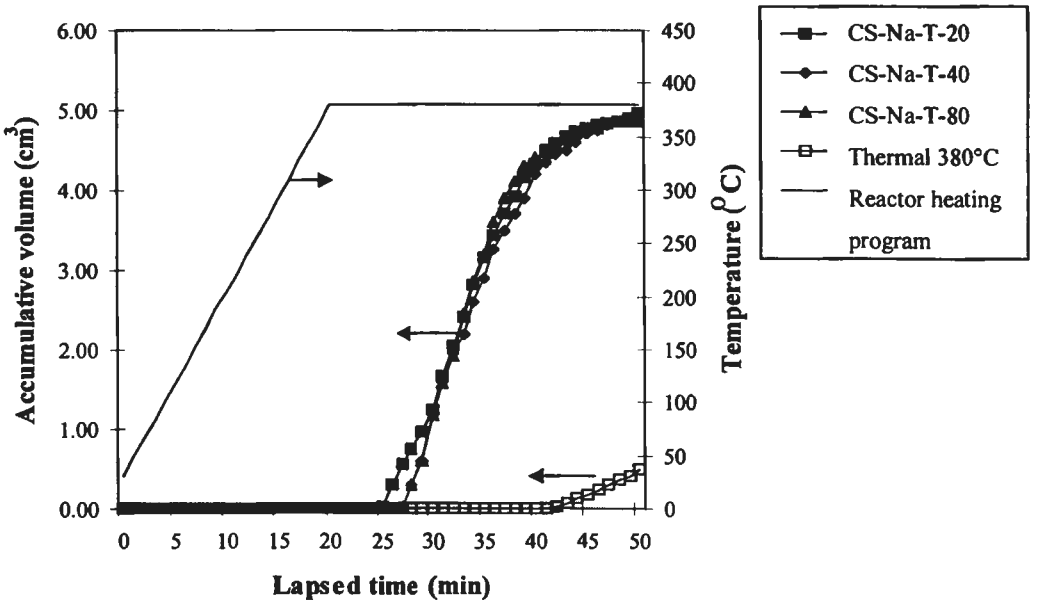

Figure 4.24 Accumulative volume of liquid fraction obtained by thermal cracking and catalytic cracking of PP over Sample CS-Na-T-20 with various Si/Al ratios at 380°C (Condition: 10 wt% catalyst of plastic, N_2 flow of 20 cm^3/min and reaction of 30 min).

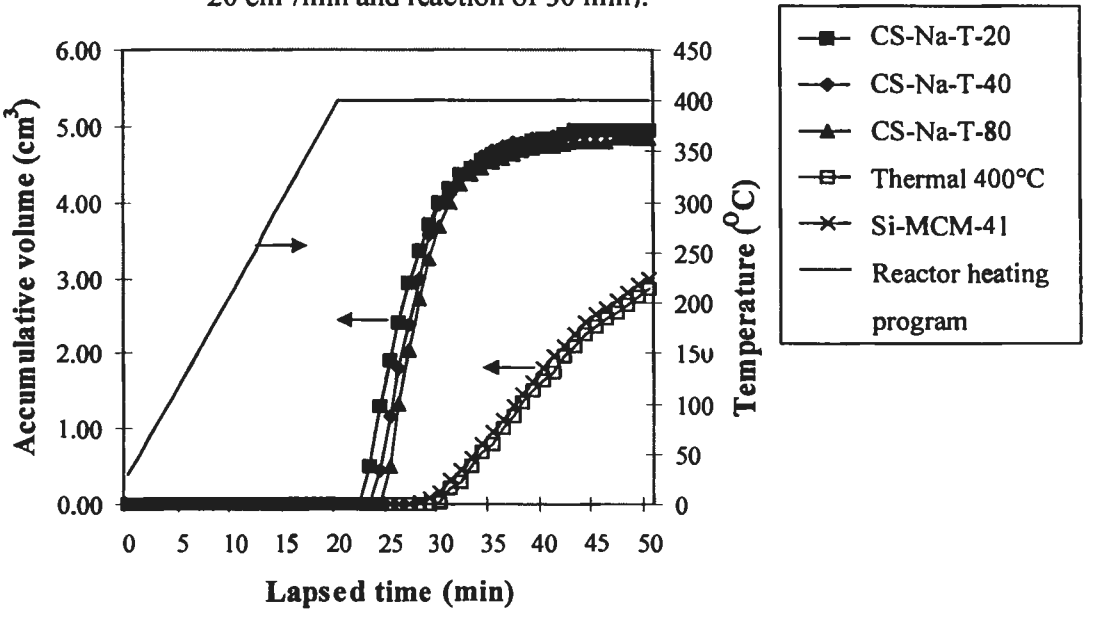

Figure 4.25 Accumulative volume of liquid fraction obtained by thermal cracking with and without non-acidic Si-MCM-41 and catalytic cracking of PP over Sample CS-Na-T-20 with various Si/Al ratios at 400°C (Condition: 10 wt% catalyst of plastic, N_2 flow of 20 cm^3/min, and reaction time of 30 min).

Figure 4.26 and Figure 4.27 shows distribution plots of gas fraction obtained by thermal cracking and catalytic cracking of PP at 380°C and 400°C, respectively. Gas fraction from catalytic cracking consists of mainly propene and i-butene, whereas the gas fraction obtained by the thermal cracking consists of propene, i-butene and n-pentane. The product distribution in gaseous phase is very slightly different upon changing the Si/Al ratio in the catalyst at both temperatures. In catalytic cracking over Si-MCM-41 the content of propene and n-pentane decreases while n-butane as well as i-butene increases. The gas fraction from the cracking over Sample CS-Na-T is rich of propene, as were the thermal cracking products.

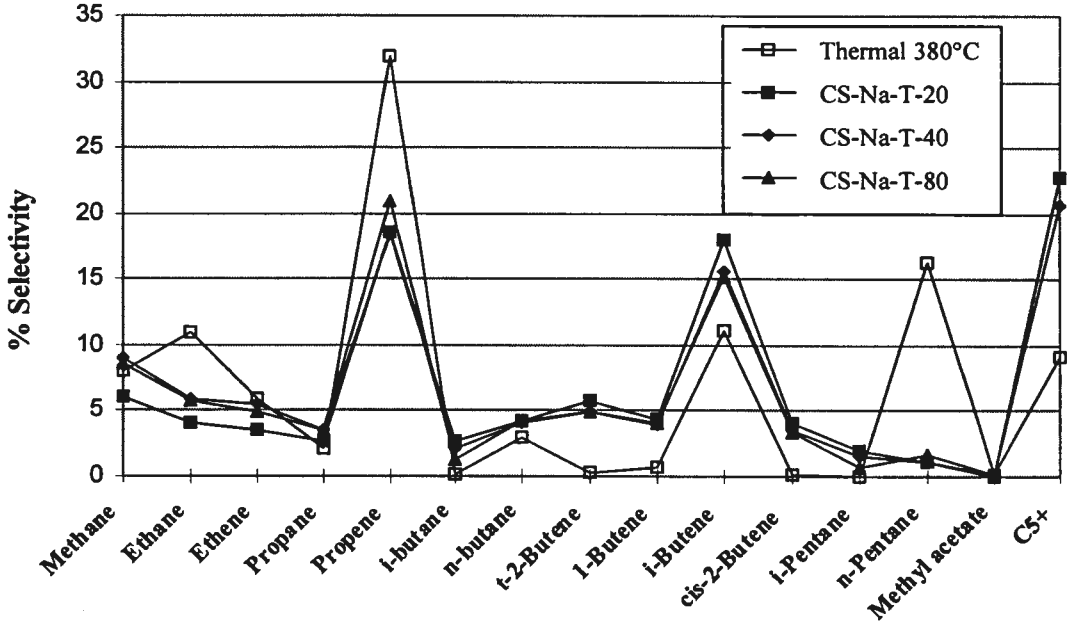

Figure 4.26 Distribution of gas fraction obtained by the thermal cracking and catalytic cracking of PP at 380°C (Condition: 10 wt% catalyst of plastic, N_2 flow of 20 cm^3/min and reaction of 30 min).

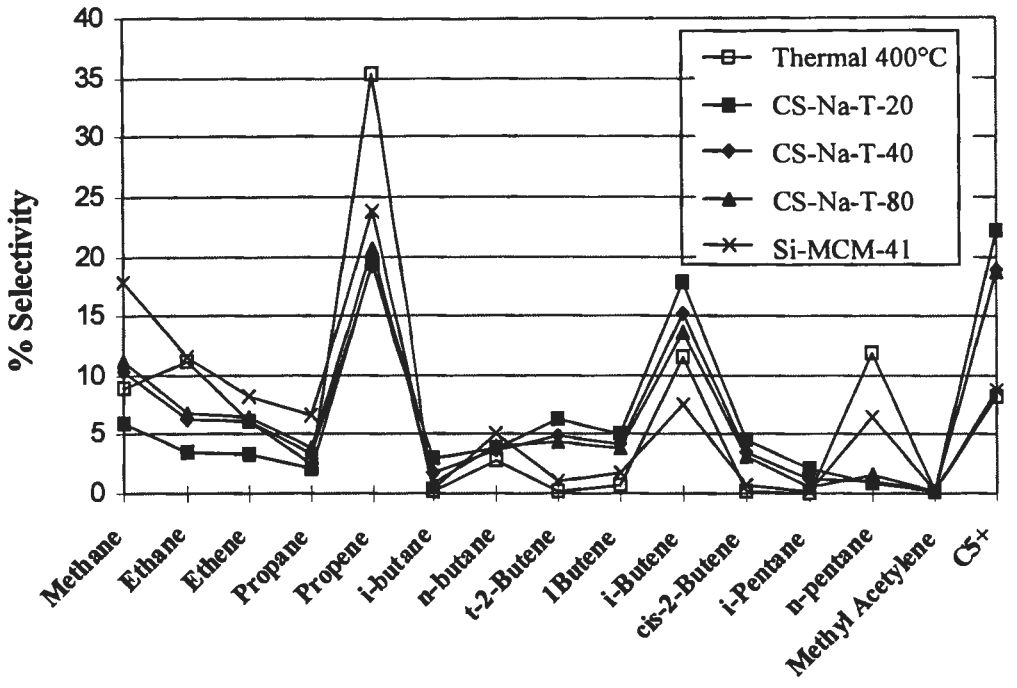

Figure 4.27 Distribution of gas fraction obtained by the thermal cracking and catalytic cracking of PP 400°C (Condition: 10 wt% catalyst of plastic, N_2 flow of 20 cm^3/min and reaction of 30 min).

Figure 4.28 and Figure 4.29 shows product distribution of distillate oil obtained by the thermal cracking and catalytic cracking of PP at 380°C and 400°C, respectively. For thermal cracking at 380°C, the liquid fraction is rich of C_9. For the thermal cracking at 400°C, the liquid hydrocarbon fractions are distributed in a wide range of equivalent hydrocarbons from C_6 to C_9. For the PP cracking over Sample CS-Na-T catalysts, the liquid fraction is rich of C_7 and C_8. When Si/Al ratio increases, the component C_8 increases. The non-acidic Si-MCM-41 is mainly C_7 through C_9. The results suggest that Al-MCM-41 as solid-acid catalyst breaks the long polymeric chain from ends into small units. It is well known that thermal cracking occurs by the random scissoring of the long polymeric chain and products of cracking are distributed in a wide range of molecular weights.

The carbon number distribution of liquid fraction obtained by catalytic cracking over Sample CS-Na-T is very similar to a commercial standard gasoline (See Figure 4.20). The distribution profile of liquid fraction obtained by the PP cracking over Si-MCM-41 locates between those by thermal cracking and by catalytic cracking over Al-MCM-41. Comparing to thermal cracking, Si-MCM-41 does not only

accelerate the rate of cracking of polymers but also degrades the heavier waxy residue into lighter liquid hydrocarbons fraction.

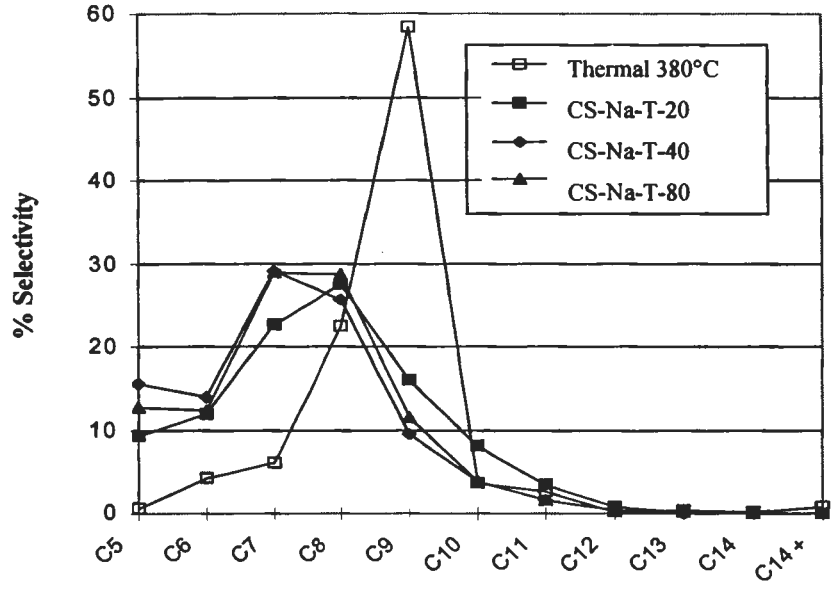

Figure 4.28 Carbon number distribution of liquid fraction from catalytic cracking of PP at 380°C (Condition: 10 wt% catalyst of plastic, N_2 flow of 20 cm^3/min and reaction of 30 min).

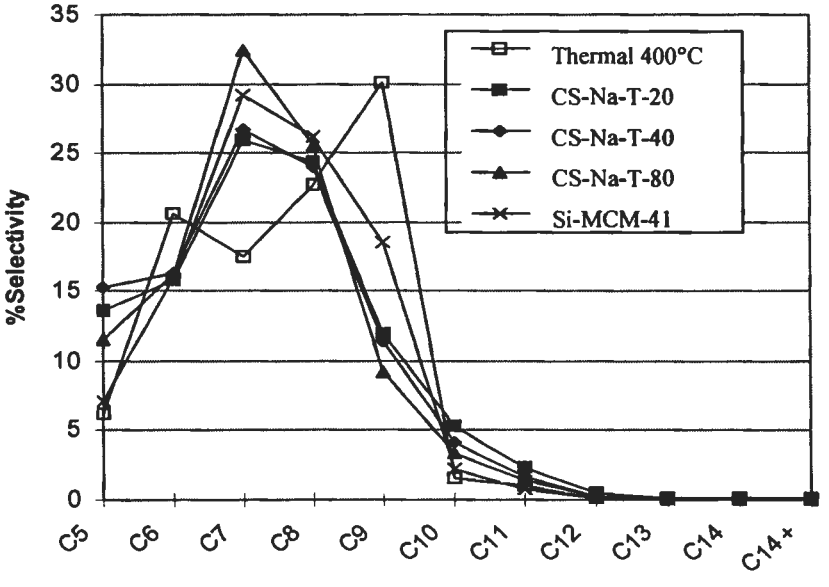

Figure 4.29 Carbon number distribution of liquid fraction from catalytic cracking of PP at 400°C (Condition: 10 wt% catalyst of plastic, N_2 flow of 20 cm^3/min and reaction of 30 min).

4.6 Catalyst Regeneration

4.6.1 XRD Results

The used Sample CS-Na-20 became black after use due to coke deposit on the surface and in the pores. However, it easily turned to white after regeneration by calcination in a muffle furnace at 540°C for 6 h. XRD patterns of the calcined unused and the regenerated Sample CS-Na-20 catalysts are shown in Figure 4.30. The hexagonal structure MCM-41 was still remained for the regenerated CS-Na-20 catalyst with almost the same crystallinity as the unused catalyst. The small shift of all three peaks to higher values of 2θ indicates the decrease of d-spacings and the contraction of the unit cell.

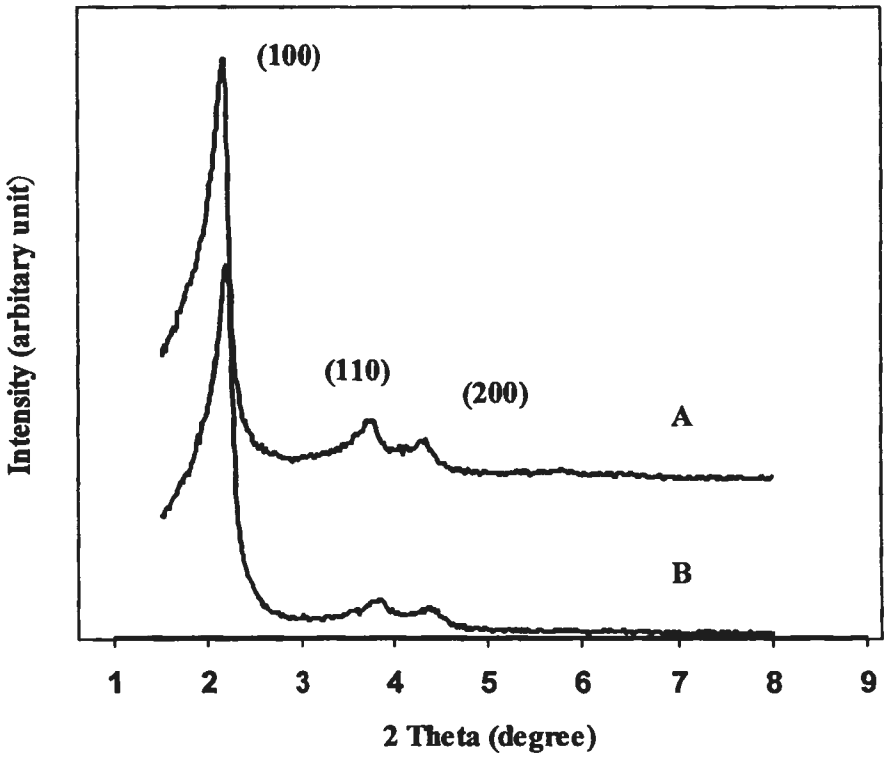

Figure 4.30 XRD patterns of (A) the calcined unused and (B) the regenerated Sample CS-Na-20 catalysts.

4.6.2 SEM Images

Figure 4.31 shows SEM images of the regenerated Sample CS-Na-T-20 catalyst prepared for SEM analysis by two different methods: dry powder method resulted in Figure 4.31 (A) and ethanolic dispersion resulted in Figure 4.31 (B). Most

particles have spherical shape and some of them have rod shape. It is obvious that the regenerated catalyst has much smaller particle size than the fresh catalyst picture of which has been shown in Figure 4.5(B).

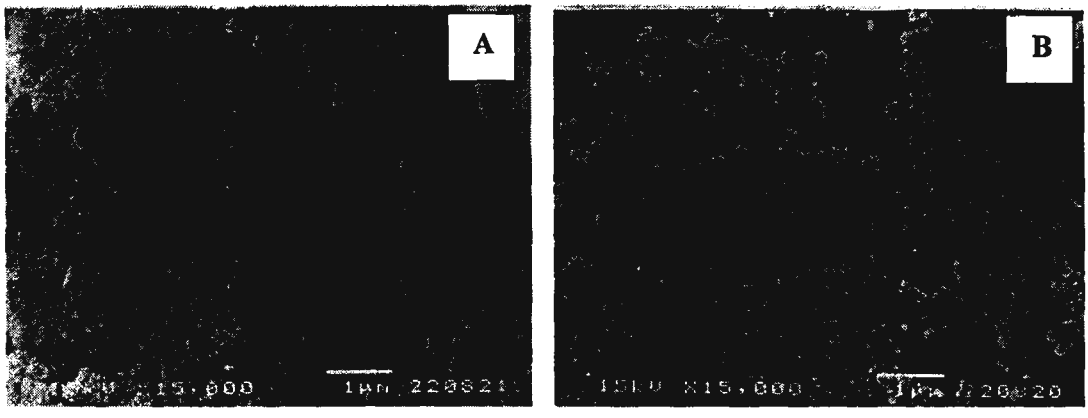

Figure 4.31 Images of regenerated Sample CS-Na-T-20 prepared for SEM analysis by (A) dry powder method and (B) ethanolic dispersion.

4.6.3 Catalytic Activity of Al-MCM-41 in PP Cracking

The values of %conversion and %yield obtained by the PP cracking using fresh and regenerated Sample CS-Na-T-20 catalysts at 400°C are shown in Table 4.8. The values of %conversion are not different and either does solid coke. The significant differences are the yield ratio of gas fraction to liquid fraction and the yield ratio of distillated oil and heavy oil. The regenerated catalyst provided relatively higher yield of gas fraction and lower yield of liquid fraction comparing to the fresh catalyst. Much higher yield of distillated oil and lower yield of heavy oil were obtained for the regenerated catalyst comparing to the fresh catalyst. This result suggests the regenerated catalyst has smaller particle size than the fresh catalyst. In other report [27], the regenerated catalyst gave higher yield of liquid fractions comparing to the fresh catalyst. The amount of liquid fractions increases from 71.1 wt% to 81.4 wt%. Relatively more amount of residue, especially in form of wax was remained in the reactor of the regenerated catalyst rather than that of fresh catalyst.

Table 4.8 Values of %conversion and %yield obtained by catalytic cracking of PP using the fresh and the regenerated Sample CS-Na-T-20 catalyst (Condition: 10 wt% catalyst of plastic, N_2 flow of 20 cm^3/min, 400 °C, and reaction time of 30 min)

	Fresh CS-Na-T-20 catalyst	Regenerated CS-Na-T-20 catalyst
%Conversion*	95.60	95.45
%Yield*		
1. gas fraction	23.50	26.14
2. liquid fraction	72.10	69.31
- % distillated oil	*59.88*	*72.28*
- % heavy oil	*40.12*	*27.72*
3. residue	4.40	4.80
- wax	*2.05*	*2.41*
- solid coke	*2.35*	*2.39*
Total volume liquid of fraction (cm^3)	4.95	4.71
Liquid fraction density (g/ cm^3)	0.7283	0.7581

*Deviation within 0.2% for conversion, 0.2% for yield of liquid fraction, and 0.2% for yield of residue.

Figure 4.32 shows the accumulative volume of liquid fraction in the graduated cylinder. The rates of liquid formation are not significantly different no matter using the fresh or the regenerated catalyst. Neither are the total amounts of liquid fraction. This shows that the catalysts can be used again at similar efficiency after regeneration.

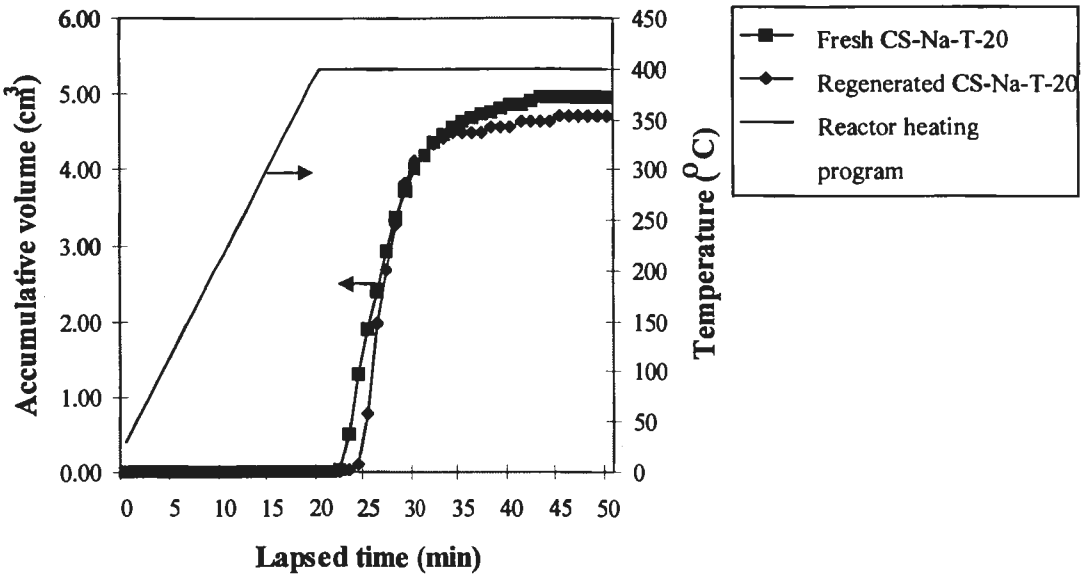

Figure 4.32 Accumulative volume of liquid fraction obtained by catalytic cracking of PP using the fresh and the regenerated Sample CS-Na-T-20 catalyst (Condition: 10 wt% catalyst of plastic, N_2 flow of 20 cm^3/min, 400 °C, and reaction time of 30 min).

Figure 4.33 shows distribution of gas fraction obtained by the PP cracking using the fresh and the regenerated Sample CS-Na-T-20 catalyst at 400°C. The gas fraction composes the same product distribution. There is no difference in selectivity in gas fraction between the two catalysts.

Figure 4.34 shows product distribution of the liquid fraction obtained by the PP cracking using the fresh and the regenerated Sample CS-Na-T-20 catalyst 400°C. Both fresh and regenerated catalysts provide mainly C_7 to C_8 range in liquid fraction. However, the selectivity to C_5 through C_8 of liquid fraction is relatively lowered when the regenerated catalyst was used.

Al-MCM-41 is stable for the use as cracking catalyst and the used catalyst can be regenerated easily in a furnace. Its cracking activity still does not change significantly.

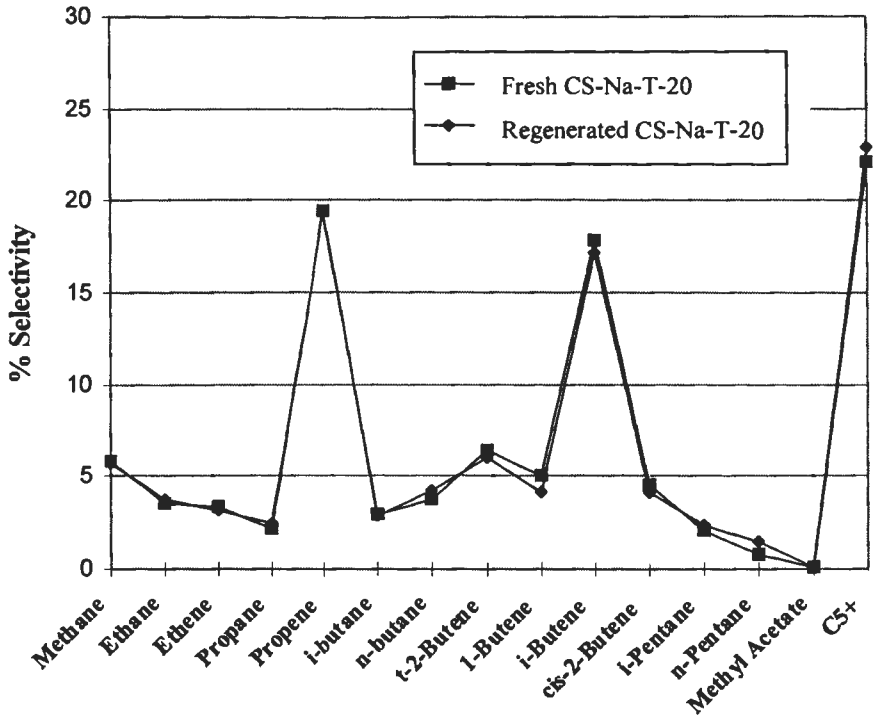

Figure 4.33 Distribution of gas fraction obtained by catalytic cracking of PP using the fresh and the regenerated Sample CS-Na-T-20 catalyst (Condition: 10 wt% catalyst of plastic, N_2 flow of 20 cm^3/min, 400 °C, and reaction time of 30 min)

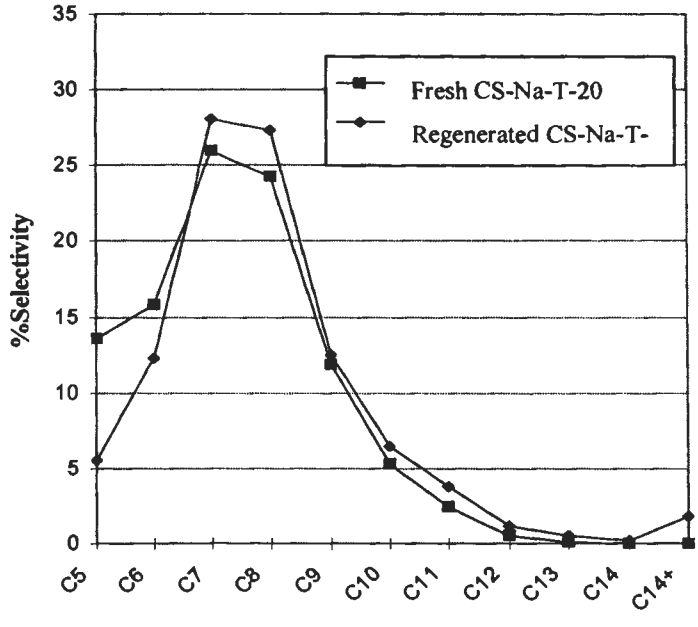

Figure 4.34 Carbon number distributions of liquid fraction obtained by catalytic cracking of PP using the fresh and the regenerated Sample CS-Na-T-20 catalyst (Condition: 10 wt% catalyst of plastic, N_2 flow of 20 cm^3/min, 400 °C, and reaction time of 30 min)